# The hierarchy of Davydov's Ansätze: from guesswork to numerically "exact" many-body wave functions

Yang Zhao

Division of Materials Science, Nanyang Technological University, Singapore 639798, Singapore

E-mail: YZhao@ntu.edu.sg

January 26, 2023

**Abstract**

This perspective presents an overview of the development of the hierarchy of Davydov's Ansätze and a few of its applications in many-body problems in computational chemical physics. Davydov's solitons originated in the investigations of vibrational energy transport in proteins in the 1970s. Momentum-space projection of these solitary waves turned up to be accurate variational ground-state wave functions for the extended Holstein molecular crystal model, lending unambiguous evidence to the absence of formal quantum phase transitions in the Holstein systems. The multiple Davydov Ansätze have been proposed, with the increasing Ansatz multiplicity, as incremental improvements of their single-Ansatz parents. For a given Hamiltonian, the time-dependent variational formalism is utilized to extract accurate dynamic and spectroscopic properties using Davydov's Ansätze as its trial states. A quantity proven to disappear for large multiplicities, the Ansatz relative deviation is introduced to quantify how closely the Schrödinger equation is obeyed. Three finite-temperature extensions to the time-dependent variation scheme are elaborated, i.e., the Monte Carlo importance sampling, the method of thermofield dynamics, and the method of displaced number states. To demonstrate the versatility of the methodology, applications of Davydov's Ansätze are made to the generalized Holstein Hamiltonian, variants of the spin-boson model, and systems of cavity-assisted singlet fission, yielding accurate dynamic and spectroscopic properties of the many-body systems.

## 1 Introduction

Alexander S. Davydov, a Ukrainian physicist from the southern suburb of Kyiv, proposed in the early 1970s a novel mechanism for transport and localization of vibrational energy in proteins stored in the form of amide I vibrations (i.e, essentially the stretching vibrations of the CO groups). It was realized early on that Davydov's theory has its roots in polaron theory [1, 2], and the jargon of Davydov's soliton was first coined in the context that vibrational energy transport in proteins is analogous to the quasiparticle movement in a polaron model in which a free electron deforms its polar crystal host, leading to a local distortion that, in turn, lowers the electron energy. [3, 4, 5]. The role of the electron in a polaron is played here by the Amide-I vibration, and its interaction

with the lattice sites is due to the dependence of the Amide-I energy on the length of the hydrogen bond that connects the CO groups. More specifically, the vibrational energy of the CO stretching (or Amide-I) oscillators, which are localized spatially on the alpha-helix of proteins, can deform the helix and cause the Amide-I oscillation energy to be trapped by acoustic modes, a process also known as self-trapping (derived from the theory of classical nonlinearity). If the deformation energy of the hydrogen-bonded lattice is lower than the reduction in the Amide-I energy, the Amide-I region is self-trapped in a state that is known as Davydov's soliton.

Initially contemplated were two Davydov's soliton, the Davydov $D_1$ and $D_2$ Ansatz, with the latter being a simplified version of the former [6, 7, 8]. Scott *et al.* have conducted experiments on crystalline acetanilide with findings analyzed using Davydov's model [9, 10]. The solitons are found to follow equations of motion (EOMs) at variance with those proposed initially by Davydov. From the very start, thermal stability of Davydov's soliton has been an issue of major concern and sustained contention in the field. Davydov first considered the temperature effects on an $\alpha$-helix soliton in 1980 [7], but his conclusion was criticized by a number of authors [1, 11]. Modifying early equations of Davydov for the $\alpha$-helix soliton, Scott claimed by numerical means that the solitary solutions may exist under physiological conditions [12]. Davydov's $D_2$ Ansatz and its thermal stability were also investigated by Förner [13, 14, 15], concluding room-temperature stability of Davydov's soliton his simulation with model parameter values that can be fulfilled in proteins. He also cited supporting arguments from several perturbative approaches and the Langevin-equation models [13]. A quantum Monte Carlo study points to classical hopping behavior of Davydov's soliton in the $\alpha$-helix at physiological temperature [16, 17], consistent with earlier finite-temperature molecular dynamics simulations [18]. Highly localized in space, a coherent structure closely resembling Davydov's soliton is found to be present at low temperatures in the quantum Monte Carlo study, but severely damaged above 7 K [16]. Despite decades of studies of Davydov's solitons, some of which are still ongoing, not much concrete evidence has been uncovered on their existence in proteins at room temperature. Nonetheless the topic of Davydov's solitons continues to fascinate and inspire a variety of workers in the field, and in some instances (as will be elaborated in this manuscript), leads to highly successful methodologies for accurate simulation of many-body quantum dynamics.

Proposed in the context of energy transport in proteins, Davydov's soliton is a spatially non-dispersing, semiclassical entity deprived of quantum signatures. As the quantum theory of polaron is linear, it is intriguing to consider how a polaronic construct such as Davydov's soliton could exhibit the behavior of a nonlinear classical system [19, 20, 21, 22, 23]. In addition, the solitary structure of Davydov's soliton is seemingly at odds with the translational invariance of the Fröhlich and the Hol-

stein Hamiltonian, of which the solitons are supposed to be approximate eigenstates. It was proven by Čápek and Krausová that delocalized, momentum-conserving states, constructed from Davydov's solitons, always have lower energies than their solitary parent states [24]. Those delocalized, momentum-conserving states are in fact the forerunners of the multiple Davydov trial states, as will be elaborated in Sec. 2. Obtained via projections onto the momentum space, momentum-conserving remakes of Davydov's solitons have gained much attention in the study of the ground-state properties of the Holstein molecular crystal model [25, 26, 27, 28, 29, 30, 31, 32, 33, 34]. For instance, the Davydov $D_2$ Ansatz, after momentum-space projection, yields celebrated Toyozawa's Ansatz [25], a fairly precise ground-state trial state of the extended Holstein Hamiltonian for most of the phase diagram except the weak coupling regime. In the mid-1980s, a delocalized, momentum-conserving state that has been simplified from Toyozawa's Ansatz to one with only two variational parameters, characterizing excitonic amplitudes and lattice distortions, was solved by Venzl and Fischer for the Holstein polaron [28], while Toyozawa's Ansatz was worked out in full by Zhao and coworkers in early 1990s, unveiling intricate details of exciton-phonon correlations inaccessible previously [29, 32]. The delocalized $D_1$ Ansatz, obtained from momentum-space projections of the Davydov $D_1$ Ansatz, is considerably more accurate than Toyozawa's Ansatz and produces results quantitatively comparable with the density matrix renormalization group (DMRG) method [34].

The multiple Davydov Ansätze, which are literally superpositions of multiple copies of the corresponding single Davydov Ansätze, encompass much more refined bosonic components in the entangled many-body trial states because of the expanded Gaussian multiplicity in their bosonic component. The multiple Davydov Ansätze were pioneered in the early 1970s by Shore and Sander when they experimented with a trial wave function with two Gaussians as its phonon component, an early forerunner of the multiple Davydov Ansätze, inspired by numerically "exact" solutions to a two-site problem with short-range coupling to Einstein phonons [27]. Also belong to the family of the multiple Davydov Ansätze are the aforementioned momentum-conserving descendents of Davydov's solitons, such as Toyozawa's Ansatz and the Global-Local Ansatz, since they are linear superpositions of $N$ copies (i.e., $N$ sites) of the corresponding single Davydov trial states. The time-independent version of the multiple Davydov $D_1$ Ansatz has recently been employed as the trial state of choice to probe a phase transition from a doubly degenerate "localized phase" to the other doubly degenerate "delocalized phase" in a sub-Ohmic spin-boson model (SBM) with both diagonal and off-diagonal spin-boson interactions, where the transition points are obtained accurately in full agreement with exact diagonalization and DMRG [35]. Time-dependent multiple Davydov Ansätze have only been deployed very recently to extract numerically "exact" many-body dynamics [36, 37]. In particular,

the multiple $D_2$ Ansatz was used to obtain high-precision polaron dynamics, resulting in efficient and accurate calculations of nonlinear spectroscopic signals [37]. Moreover, the SBM phase diagram of the dynamical coherent-incoherent crossover was also established by the multiple $D_1$ Ansatz [36]. A number of authors in the field have utilized the multiple $D_2$ Ansatz to handle Hamiltonians with bilinear particle-boson coupling [38, 39, 40], and collectively, their results seem to conclude that the multiple $D_2$ Ansatz alone can provide sufficiently accurate descriptions to the many-body quantum dynamics in the presence of nonlinearity, with only negligible benefits from extending the multi-D2 Ansatz to include squeezing effects.

Traditionally, the density matrix formalism is known to be a straightforward approach to multidimensional spectroscopic signals. Via propagating the reduced density matrix along various Liouville pathways, nonlinear response functions can be readily determined [41]. In this regard, the numerically "exact" approaches of hierarchical equations of motion (HEOM) [42, 43] and the quasiadiabatic path integral (QUAPI) [44, 45] are among the best known for nonlinear spectra computation [46, 47, 48, 49], despite that both are computationally prohibitive at low temperatures and in the regime of strong system-bath coupling. Moreover, the HEOM construction confines its applications to certain bath spectral densities [50, 51, 52]. Wave function-based approaches offer an alternative to the density matrix formalism for deriving nonlinear responses. Examples of wave function-based methods include the multiconfiguration time-dependent Hartree (MCTDH) method and its multilayer extension (ML-MCTDH) [53, 54, 55, 56], the multiple spawning (MS) method [57, 58], the hierarchy of Davydov's Ansätze (HDA) [59, 60, 37, 61, 62, 63, 64], and other basis set methods [65, 66, 67, 68, 69, 70], delivering accurate dynamics descriptions for all temperatures. A few useful techniques are available to extract finite-temperature dynamics and spectra from the wave function-based HDA approach, including the well known Monte Carlo importance sampling to initialize vibrational modes [71, 72], the method of displaced number states to take advantage of the fact that initial excitation of the nuclear manifold can be conveniently expressed by bath displaced number states [73, 74], and the thermofield dynamics (TFD) approach to map the Liouville-von Neumannn equation to the corresponding TFD Schrödinger equation with twice the bath size [75, 76, 77, 78, 79, 80, 81, 82, 83]. The performance of the ML-MCTDH approach has been compared with that of the HDA method by a very recent study [84], demonstrating a few computational advantages of the HDA method.

The remainder of this Perspective is structured as follows. Sec. 2 of this Perspective centers on the historical development of the family of the Davydov's Ansätze, i.e., from semiclassical Davydov's solitons and single Davydov Ansätze [85, 86] to their multistate extensions [60, 37, 62, 36]. In Sec. 3, using the multi-$D_2$ Ansatz as an example, the time-dependent variational formalism of Davydov's

Ansätze is given, and relative deviations of the Ansätze are defined to track the accuracy of the trial states. In Sec. 4 elaborates on three techniques, Monte Carlo importance sampling, the method of displaced number states, and the TFD approach, to extend the HDA methodology to finite-temperature dynamics of many-body systems. Sec. 5 describes how nonlinear response functions and various spectroscopic signals are computed via propagating Davydov's Ansätze in time. The HDA approach has been extensively applied to accurate simulation of quantum dynamics of many-body systems and the corresponding spectroscopic manifestations [60, 37, 72, 79, 85, 86, 36, 87, 88, 89], which is reviewed next in Secs. 6 to 8 of the Perspective. Conclusions and discussion are presented in Sec. 9.

## 2 The family of Davydov's Ansätze

As a quasi-classical entity, Davydov's soliton is demonstrated, under certain approximations, to obey the nonlinear Schrödinger equation often seen in soliton studies [90]. Davydov's starting point is the Holstein molecular crystal model in which intramolecular excitations are linearly coupled to molecular modes. The extended Holstein Hamiltonian in one dimension, $\hat{H}^{\rm ext}_{\rm Holstein}$, also known as the generalized Holstein molecular crystal model, reads in the momentum space,

$$\begin{aligned} \hat{H}^{\rm ext}_{\rm Holstein} &= \sum_k J_k a_k^\dagger a_k + \sum_q \omega_q b_q^\dagger b_q + \hat{H}_{\rm ex-ph}, \\ \hat{H}^{\rm ext}_{\rm ex-ph} &= N^{-1/2} \sum_{kq} \omega_q f^q_{-k} a^\dagger_{k+q} a_k (b_q + b^\dagger_{-q}), \end{aligned} \tag{1}$$

where $\hbar = 1$, $\omega_q$ is the frequency of $q$th mode, and $a_k^\dagger$, $b_q^\dagger$ ($a_k$, $b_q$) are the exciton and phonon creation (annihilation) operators of wave vectors $k$ and $q$, respectively. $J_k$ is the momentum-space transfer integral. $\hat{H}^{\rm ext}_{\rm ex-ph}$ is the coupling Hamiltonian with $f^q_k$ being the linear coupling strength. $\hat{H}^{\rm ext}_{\rm Holstein}$ has been frequently applied to quasi-one-dimensional solids that are characterized by considerable anisotropy in their transport properties. Hamiltonian (1) is closely associated with the concept of a polaron, a quasiparticle excitation clothed by deformation or polarization quanta of a solid [91]. On the other hand, Davydov's solitons may be viewed as particle-like solutions to nonlinear Schrödinger equation that are connected to the polarons in the correspondence limit [92]. While it is likely that the polarons may be quantum solitary waves, Davydov's solitons serve as asymptotic forms of the polaron in the adiabatic limit [32].

Non-dispersing (and non-dissipating) over long distances, Davydov's solitons are solitary waves that are tasked to capture the essence of seemingly soliton-like transport in proteins. Translationally invariant Hamiltonians, such as the aforementioned Holstein Hamiltonian, often have trial wave

functions with similar translational symmetries for their ground states. In order to extract accurate variational wave functions for those Hamiltonians, Davydov's solitons need to be projected onto the crystal-momentum space. To illustrate the projection procedure, we show how to convert a wave function, $a_0^\dagger e^{-\sum_{n_2}(\delta_{n_2}^K b_{n_2}^\dagger - \delta_{n_2}^{K*} b_{n_2})}|0\rangle$, which is centered at site $n = 0$ with a product of Glauber coherent states [93], to a translationally invariant trial state

$$|\Psi_{\rm small}^K\rangle = N^{-\frac{1}{2}} \sum_n e^{iKn} a_n^\dagger \exp[-\sum_{n_2}(\delta_{n_2-n}^K b_{n_2}^\dagger - \delta_{n_2-n}^{K*} b_{n_2})]\ |0\rangle, \tag{2}$$

where $|0\rangle$ is the vacuum state of both the exciton and the phonons, and $\delta_n^K$ stands for phonon displacements. Ansatz (2), called the "small polaron Ansatz $|\Psi_{\rm small}^K\rangle$," is constructed by applying the projection operator

$$\hat{\Xi}(K) = N^{-1} \sum_n e^{i(K-\hat{P})n}, \tag{3}$$

characterized by parameter $K$ and the crystal momentum operator $\hat{P} = \sum_k k a_k^\dagger a_k + \sum_q q b_q^\dagger b_q$. The projection operator (3) produces a sum of $n$ site-space structures (i.e., Davydov's solitons) displaced from the origin by $n$ lattice spacings, and weighted by a factor of $e^{iKn}$.

Toyozawa proposed a momentum-conserving trial state in 1961 [25], which is known as Toyozawa's Ansatz:

$$|\Psi_{\rm Toyozawa}^K\rangle = N^{-\frac{1}{2}} \sum_n e^{iKn} \sum_{n_1} \psi_{n_1-n}^K a_{n_1}^\dagger \exp[-\sum_{n_2}(\lambda_{n_2-n}^K b_{n_2}^\dagger - \lambda_{n_2-n}^{K*} b_{n_2})]|0\rangle. \tag{4}$$

Here $\lambda_n^K$ again represents the phonon deformation, and $\psi_n^K$ is the exciton amplitude capturing the electronic excitation distribution. Toyozawa's Ansatz can also be derived by making translationally invariant the so-called Davydov "$D_2$" Ansatz in the theory of Davydov's solitons

$$|\Psi_{\rm D_2}\rangle = \sum_{n_1} \psi_{n_1}^K a_{n_1}^\dagger \exp[-\sum_{n_2}(\lambda_{n_2}^K b_{n_2}^\dagger - \lambda_{n_2}^{K*} b_{n_2})]|0\rangle \tag{5}$$

by the application of $\hat{\Xi}(K)$. In contrast to the state $|\Psi_{\rm small}^K\rangle$ with its electronic excitation localized on one site, Davydov's $D_2$ Ansatz allows for the electronic excitation to adapt to the phonon deformation in a self-consistent manner. However, the $D_2$ Ansatz does not have an explicit exciton-phonon correlation, as $n_1$ and $n_2$ are independent of each other. The question of whether such an explicit correlation is important for capturing the ground-state properties of Hamiltonian (2) may be answered by considering the Davydov "$\tilde{\rm D}$" Ansatz, a more general trial state that was introduced by Ivić *et al.* [94]:

$$|\Psi_{\tilde{\rm D}}\rangle = \sum_{n_1} \psi_{n_1}^K a_{n_1}^\dagger \exp\{-\sum_{n_2}[(\alpha_{n_2}^K - \beta_{n_2-n_1}^K) b_{n_2}^\dagger - {\rm H.c.}]\}|0\rangle, \tag{6}$$

where the new addition $\beta_n^K$ provides a direct exciton-phonon correlation, and H.c. denotes Hermitian conjugate. Eq. (6) sits midway between Davydov's $D_2$ Ansatz and the so-called "$D_1$" Ansatz in Davydov's soliton theory:

$$|\Psi_{\mathrm{D}_1}\rangle = \sum_{n_1} \psi_{n_1}^K a_{n_1}^\dagger \exp[-\sum_{n_2}(\gamma_{n_2,n_1}^K b_{n_2}^\dagger - \mathrm{H.c.})]|0\rangle. \tag{7}$$

In Eq. (7), the phonon-structure dependence on $n_1$ in the Davydov "D1" Ansatz is captured by the triple-indexed variational parameter $\gamma_{n_2,n_1}^K$. In contrast, in Eq. (6), this dependence is represented solely by $\beta_{n_2-n_1}^K$.

Momentum-space projection of Eq. (6) leads to the delocalized Davydov "$\tilde{\mathrm{D}}$" Ansatz [86], also known in the literature as the Global-Local Ansatz [33]

$$|\Psi_{\mathrm{GL}}^K\rangle = N^{-\frac{1}{2}} \sum_n e^{iKn} \sum_{n_1} \psi_{n_1-n}^K a_{n_1}^\dagger \exp\{-\sum_{n_2}[(\alpha_{n_2-n}^K - \beta_{n_2-n_1}^K) b_{n_2}^\dagger - H.c.]\}|0\rangle, \tag{8}$$

Correspondingly, momentum-space projection of the Davydov "$D_1$" Ansatz yields the delocalized Davydov "$D_1$" Ansatz [34]

$$|\Psi_{\mathrm{dD}_1}^K\rangle = N^{-\frac{1}{2}} \sum_n e^{iKn} \sum_{n_1} \psi_{n_1-n}^K a_{n_1}^\dagger \exp\{-\sum_{n_2}[\gamma_{n_2-n,n_1-n}^K b_{n_2}^\dagger - H.c.]\}|0\rangle, \tag{9}$$

Here $\psi_n^K$ represent coefficients in a linear combination of Gaussian states if Eq. (4) is recast as follows [95]:

$$|\Psi_{\mathrm{Toyozawa}}^K\rangle = N^{-\frac{1}{2}} \sum_n e^{iKn} a_n^\dagger \sum_{n_1} e^{-iKn_1} \psi_{n_1}^K \exp[-\sum_{n_2}(\lambda_{n_2+n_1-n}^K b_{n_2}^\dagger - \lambda_{n_2+n_1-n}^{K*} b_{n_2})]|0\rangle.$$

Correspondingly, the Global-Local Ansatz (8) may also be recast as

$$|\Psi_{\mathrm{GL}}^K\rangle = N^{-\frac{1}{2}} \sum_n e^{iKn} a_n^\dagger \sum_{n_1} e^{-iKn_1} \psi_{n_1}^K \exp\{-\sum_{n_2}[(\alpha_{n_2+n_1-n}^K - \beta_{n_2-n}^K) b_{n_2}^\dagger - H.c.]\}|0\rangle,$$

where the variational parameter $\beta_{n_2-n}^K$ is seen to represent a phonon component independent of $n_1$.

Next, we proceed to introduce the latest addition to the hierarchy of Davydov trial states, the multiple Davydov Ansätze. The two-site SBM will be utilized as an example to illustrate how the familiar single Davydov Ansätze may be generalized to adopt a linear combination of Gaussian states, and as a consequence, the accuracy of the resultant trial wave functions will be substantially improved in dynamics studies of many-body systems. The multiple Davydov's Ansätze of the two-site SBM can be easily generalized to those of a multiple-site Hamiltonian, as will be elaborated toward the end of Sec. 2.

The SBM Hamiltonian, $\hat{H}_{\rm SBM}$, reads

$$\hat{H}_{\rm SBM} = \frac{\epsilon}{2}\sigma_z - \frac{\Delta}{2}\sigma_x + \sum_l \omega_l b_l^\dagger b_l + \frac{\sigma_z}{2}\sum_l \lambda_l (b_l^\dagger + b_l), \tag{10}$$

where $\epsilon$ and $\Delta$ are the bias and the tunneling constant, respectively, $\sigma_i$ $(i = x, z)$ are Pauli operators, $\sigma_x = |+\rangle\langle -| + |-\rangle\langle +|$ and $\sigma_z = |+\rangle\langle +| - |-\rangle\langle -|$ with $|+\rangle$ and $|-\rangle$ labeling two localized electronic states. $b_l^\dagger$ $(b_l)$ is the creation (annihilation) operator for the $l$th mode, and $\omega_l$ and $\lambda_l$ are the frequency and the coupling strength of the $l$th mode, respectively. First, the two-site Davydov $\mathrm{D}_1$ Ansatz may be replaced by its multiple variant $|\Psi_{\mathrm{D}_1}^M(t)\rangle$, also known as the multi-$\mathrm{D}_1$ Ansatz with mulplicity $M$, as follows

$$|\Psi_{\mathrm{D}_1}^M(t)\rangle = \sum_u^M A_u(t)|+\rangle \exp(\sum_l f_{ul}(t) b_l^\dagger - \mathrm{H.c.})|0\rangle_{\rm ph} + \sum_u^M B_u(t)|-\rangle \exp(\sum_l g_{ul}(t) b_l^\dagger - \mathrm{H.c.})|0\rangle_{\rm ph} \tag{11}$$

Here $|+\rangle(|-\rangle)$ is the spin-up (spin-down) state, and $|0\rangle_{\rm ph}$ is the bath vacuum state. $A_u(t), B_u(t)$ are the amplitudes of $|+\rangle$ and $|-\rangle$, respectively, and $f_{ul}(t)$ and $g_{ul}(t)$ are the corresponding bosonic deformations, where $u$ and $l$ denotes the $u$th Gaussian superposition and the $l$th mode, respectively. Next, the multiple variant of the Davydov $\mathrm{D}_2$ Ansatz, also known as the multi-$\mathrm{D}_2$ Ansatz, is given by

$$|\Psi_{\mathrm{D}_2}^M(t)\rangle = \sum_u^M [A_u(t)|+\rangle + B_u(t)|-\rangle] \exp(\sum_l f_{ul}(t) b_l^\dagger - \mathrm{H.c.})|0\rangle_{\rm ph} \tag{12}$$

A trial state with its complexity sandwiched between those of the Davydov $\mathrm{D}_1$ and $\mathrm{D}_2$ Ansatz, the Davydov $\mathrm{D}_{1.5}$ Ansatz [96] can also be generalized to form the multi-$\mathrm{D}_{1.5}$ Ansatz of multiplicity $M$,

$$|\Psi_{\mathrm{D}_{1.5}}^M(t)\rangle = \sum_u^M A_u(t)|+\rangle e^{(\sum_l (f_{ul}(t) - N_l) b_l^\dagger - \mathrm{H.c.})}|0\rangle_{\rm ph} + \sum_u^M B_u(t)|-\rangle e^{(\sum_l (f_{ul}(t) + N_l) b_l^\dagger - \mathrm{H.c.})}|0\rangle_{\rm ph} \tag{13}$$

where $N_l = \lambda_l / 2\omega_l$. Similar generalizations can be made to the two-site Davydov $\tilde{\mathrm{D}}$ Ansatz.

The multi-$\mathrm{D}_2$ Ansatz is seen as a simplified form of the multi-$\mathrm{D}_1$ Ansatz of the same multiplicity, since the boson component in the former is identical for the up and down spin states. But upon closer examination of Eq. (12), it becomes clear that the multi-$\mathrm{D}_1$ Ansatz is also a special case of the multi-$\mathrm{D}_2$ Ansatz of twice the multiplicity, with $A_u(t) = 0$ for even $u$, and $B_u(t) = 0$ for odd $u$. In Sec. 6.4, a numerical comparison of a multi-$\mathrm{D}_1$ Ansatz ($M = 3$) and a corresponding multi-$\mathrm{D}_2$ Ansatz with twice the multiplicity ($M = 6$) is given explicitly for the problem of a qubit simultaneously coupled to a microcavity and a radiation bath. The multi-$\mathrm{D}_{1.5}$ Ansatz, on the other hand, is sandwiched by the two aforementioned multiple Davydov trial states of the same multiplicity on the scale of complexity.

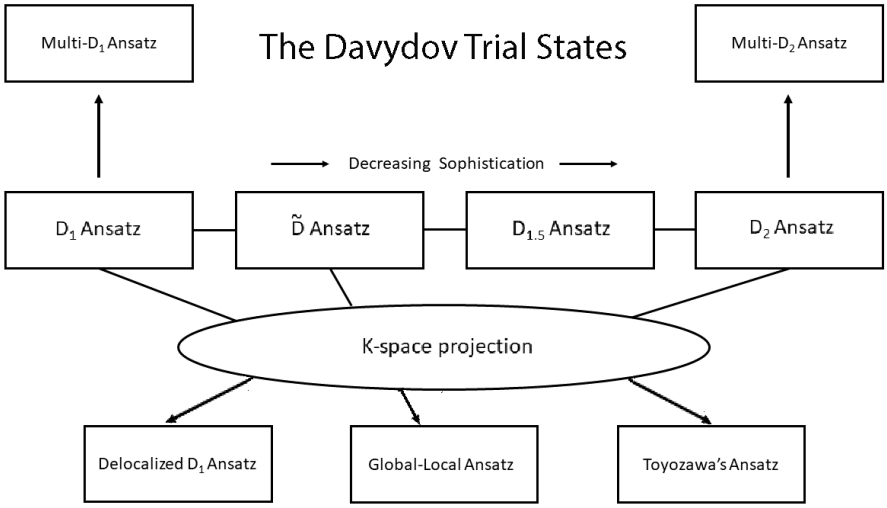


Figure 1: Schematic of the family of Davydov trial states. Top row: the multi-$\mathrm{D}_1$ Ansatz and the multi-$\mathrm{D}_2$ Ansatz. Second row: the $\mathrm{D}_1$ Ansatz, the $\tilde{\mathrm{D}}$ Ansatz, the $\mathrm{D}_{1.5}$ Ansatz, and the $\mathrm{D}_2$ Ansatz, in the order of decreasing complexity. Bottom row: momentum-conserving Davydov Ansätze, in the order of decreasing complexity (from left to right).

Lastly, the multiple-site Hamiltonian (1) may be handled numerically to any desired accuracy by replacing Eqs. (5) and (7) with their respective multiple trial state extensions, given sufficiently large Ansatz multiplicities [60, 37]. The multiple-site (or multiple-state) multi-$\mathrm{D}_1$ Ansatz of multiplicity $M$ reads [37, 62]

$$|\Psi^M_{\mathrm{D}_1}(t)\rangle = \sum_m |m\rangle \sum_{k=1}^{M} A_{mk}(t) e^{\left(\sum_l f_{m,kl}(t) b_l^\dagger - \mathrm{H.c.}\right)} |0\rangle_{\mathrm{ph}}, \tag{14}$$

where $|m\rangle$ denotes the $m$th excitation site (state) of a multiple-site (multiple-state) system with $f_{m,kl}(t)$ being the corresponding phonon field component for the $l$th phonon mode in the $k$th coherent-state superposition (with a total of $M$ superpositions). The multiple-site (or multiple-state) version for the multi-$\mathrm{D}_2$ Ansatz of multiplicity $M$ reads [37, 38]

$$|\Psi^M_{\mathrm{D}_2}(t)\rangle = \sum_m |m\rangle \sum_{k=1}^{M} A_{mk}(t) e^{\left(\sum_l g_{kl}(t) b_l^\dagger - \mathrm{H.c.}\right)} |0\rangle_{\mathrm{ph}}, \tag{15}$$

where $g_{kl}(t)$ is the phonon field component for the $l$th phonon mode in the $k$th coherent-state superposition (with a total of $M$ superpositions). In the sections to come, $|\mathrm{D}^M_{1,2}\rangle$ is used to refer to $|\Psi^M_{\mathrm{D}_{1,2}}\rangle$.

Fig. 1 displays a schematic diagram of the family of Davydov trial states, which illustrates the hierarchy of Davydov's Ansätze and the intertwined relations among the states. The second row

from the top contains four Davydov's solitons, in the order of decreasing complexity, the $D_1$ Ansatz, the $\tilde{D}$ Ansatz, the $D_{1.5}$ Ansatz, and the $D_2$ Ansatz, all of which are spatially localized. Projection of Davydov's solitons onto the crystal-momentum space gives rise to the momentum conserving Davydov trial states, i.e., the delocalized $D_1$ Ansatz, the Global-Local Ansatz, and Toyozawa's Ansatz, again in the order of decreasing sophistication, which are displayed in the bottom row. There are two multiple Davydov Ansätze in the top row, the multi-$D_1$ and the multi-$D_2$ Ansatz, both of which have been shown to be workhorses in the accurate dynamics simulation of a variety of many-body systems [39, 97, 98], producing numerically "exact" solutions to the Schrödinger equations.

## 3 Time-Dependent Variation of Davydov's Ansätze

Employing the example of the multi-$D_2$ Ansatz (15), we demonstrate in this section how to derive EOMs for the variational parameters of a Davydov Ansatz according to the principle of time-dependent variation. The time dependence of the variational parameters $\mu_i$ follows the Euler equations below,

$$\frac{d}{dt}\frac{\partial L}{\partial \dot{\mu}_i^*} - \frac{\partial L}{\partial \mu_i^*} = 0, \tag{16}$$

where the Lagrangian is constructed as

$$L = \frac{i}{2}\left[\langle \mathrm{D}_2^M(t)|\frac{\overrightarrow{\partial}}{\partial t}|\mathrm{D}_2^M(t)\rangle - \langle \mathrm{D}_2^M(t)|\frac{\overleftarrow{\partial}}{\partial t}|\mathrm{D}_2^M(t)\rangle\right] - \langle \mathrm{D}_2^M(t)|H|\mathrm{D}_2^M(t)\rangle =: L_{\mathrm{td}} - L_{\mathrm{H}}. \tag{17}$$

Using the Davydov-Ansatz normalization, the time derivative needs only to be taken to the right. Thus, the first term in Eq. (17), $L_{\mathrm{td}}$, is given by

$$L_{\mathrm{td}} = i\langle \mathrm{D}_2^M(t)|\frac{\overrightarrow{\partial}}{\partial t}|\mathrm{D}_2^M(t)\rangle = i\sum_m \sum_{k,p}^M A_{mk}^* S_{kp}\left(\dot{A}_{mp} + A_{mp}\sum_q \frac{2f_{kq}^*\dot{f}_{pq} - f_{pq}^*\dot{f}_{pq} - f_{pq}\dot{f}_{pq}^*}{2}\right), \tag{18}$$

where $S_{kp} = \exp\sum_q\left\{-\left(|f_{kq}|^2 + |f_{pq}|^2\right)/2 + f_{kq}^* f_{pq}\right\}$. The second term in Eq. (17), $L_{\mathrm{H}}$, is the average system energy,

$$\begin{aligned} L_{\mathrm{H}} &= \left\langle \mathrm{D}_2^M(t)\right| H \left|\mathrm{D}_2^M(t)\right\rangle \\ &= \sum_m \sum_{k,p}^M \epsilon_m A_{mk}^* A_{mp} S_{kp} + \sum_m \sum_{m'\neq m} \sum_{k,p}^M J_{mm'} A_{mk}^* A_{m'p} S_{kp} \\ &\quad + \sum_m \sum_{k,p}^M A_{mk}^* A_{mp} \sum_q \omega_q f_{kq}^* f_{pq} S_{kp} + \sum_m \sum_{m'} \sum_{k,p}^M \sum_q g_q^{mm'} A_{mk}^* A_{m'p}\left(f_{pq} + f_{kq}^*\right) S_{kp}. \end{aligned} \tag{19}$$

We arrive at he EOMs governing $A_{mp}$,

$$
\begin{aligned}
&i\sum_{p}^{M}\dot{A}_{mp}S_{kp}+i\sum_{p}^{M}A_{mp}\sum_{q}\left[-\frac{1}{2}\left(\dot{f}_{pq}f_{pq}^{*}+f_{pq}\dot{f}_{pq}^{*}\right)+f_{kq}^{*}\dot{f}_{pq}\right]S_{kp}\\
&=\epsilon_{m}\sum_{p}^{M}A_{mp}S_{kp}+\sum_{m'\neq m}\sum_{p}^{M}J_{mm'}A_{m'p}S_{kp}+\sum_{p}^{M}A_{mp}\sum_{q}\omega_{q}f_{kq}^{*}f_{pq}S_{kp}\\
&+\sum_{p}^{M}A_{mp}\sum_{q}g_{q}^{mm}\left(f_{pq}+f_{kq}^{*}\right)S_{kp}+\sum_{m'\neq m}\sum_{p}^{M}A_{m'p}\sum_{q}g_{q}^{mm'}\left(f_{pq}+f_{kq}^{*}\right)S_{kp}.
\end{aligned}
\tag{20}
$$

Correspondingly, the EOMs for $f_{pq}$ are given as

$$
\begin{aligned}
&i\sum_{m}\sum_{p}^{M}A_{mk}^{*}\dot{A}_{mp}f_{pq}S_{kp}+i\sum_{m}\sum_{p}^{M}A_{mk}^{*}A_{mp}\dot{f}_{pq}S_{kp}\\
&+i\sum_{m}\sum_{p}^{M}A_{mk}^{*}A_{mp}f_{pq}S_{kp}\sum_{q'}\left[f_{kq'}^{*}\dot{f}_{pq'}-\frac{1}{2}\left(\dot{f}_{pq'}f_{pq'}^{*}+f_{pq'}\dot{f}_{pq'}^{*}\right)\right]\\
&=\sum_{m}\sum_{p}^{M}\epsilon_{m}A_{mk}^{*}A_{mp}f_{pq}S_{kp}+\sum_{m}\sum_{m'\neq m}\sum_{p}^{M}J_{mm'}A_{mk}^{*}A_{m'p}f_{pq}S_{kp}\\
&+\sum_{m}\sum_{p}^{M}A_{mk}^{*}A_{mp}\omega_{k}f_{pq}S_{kp}+\sum_{m}\sum_{p}^{M}f_{pq}\sum_{q'}A_{mk}^{*}A_{mp}\omega_{q'}f_{kq'}^{*}f_{pq'}S_{kp}\\
&+\sum_{m}\sum_{m'}\sum_{p}^{M}A_{mk}^{*}A_{m'p}g_{q}^{mm'}S_{kp}+\sum_{m}\sum_{m'}\sum_{p}^{M}f_{pq}\sum_{q'}A_{mk}^{*}A_{m'p}g_{q'}^{mm'}\left(f_{pq'}+f_{kq'}^{*}\right)S_{kp}.
\end{aligned}
\tag{21}
$$

To bypass singularity, uniformly distributed noise (within $[-10^{-5},10^{-5}]$) is used to initialize the variational parameters $A_{mk}$ and $f_{kl}$. Eqs. (20) and (21) compose a set of linear differential equations, in the form of $\mathbf{A}\dot{\vec{x}}=\mathbf{B}$, to be solved by the fourth-order Runge Kutta method.

In addition, to gauge the effectiveness of the multi-$\mathrm{D}_{1,2}$ Ansatz, a measure called "relative deviation" may be introduced. If a trial state $|\mathrm{D}_{2}^{M}(t)\rangle$ is to approximate the exact wave function $|\Psi(t)\rangle$ at time $t$ , we may define a deviation vector $|\vec{\delta}(t)\rangle$ to quantify the accuracy of the variational dynamics based on the multiple Davydov trial states,

$$
|\vec{\delta}(t)\rangle=-i\hat{H}|\mathrm{D}_{1,2}^{M}(t)\rangle-\frac{\partial}{\partial t}|\mathrm{D}_{1,2}^{M}(t)\rangle. \tag{22}
$$

If the trial wave function is exact (i.e., $|\Psi(t)\rangle=|\mathrm{D}_{1,2}^{M}(t)\rangle$), and therefore obeys the Schrödinger equation, then $|\vec{\delta}(t)\rangle$ vanishes. Thus, the deviation of variation dynamics of the multi-$\mathrm{D}_{1,2}$ Ansatz from the exact Schrödinger dynamics can be quantified by the amplitude of the deviation vector

$\Delta(t) = |||\vec{\delta}(t)\rangle||$. To better compare the deviation in the parameter space, a dimensionless "relative deviation" $\sigma$ is evaluated as

$$\sigma = \frac{\max\{\Delta(t)\}}{\text{mean}\{N_{\text{err}}(t)\}}, \qquad t \in [0, t_{\max}]. \tag{23}$$

where $N_{\text{err}}(t)$ is the amplitude of the time derivative of $|\mathrm{D}_{1,2}^{M}(t)\rangle$, given approximately by

$$N_{\text{err}}(t) = \sqrt{\langle \frac{\partial}{\partial t}\mathrm{D}_2^M | \frac{\partial}{\partial t}\mathrm{D}_2^M \rangle} = \sqrt{\langle \mathrm{D}_{1,2}^M(t) | \hat{H}^2 | \mathrm{D}_{1,2}^M(t)\rangle}. \tag{24}$$

# 4 Simulation of spectroscopic signals

Over the past few decades, multidimensional spectroscopy has emerged as an essential apparatus for studying energy/charge transfer in a wide range of novel materials [99, 100]. Unlike linear spectral techniques, which often has congested spectral lines, nonlinear spectroscopy allows for the use of multiple laser interactions to distinguish between dynamic processes that occur on different time scales. Understanding the spectroscopic manifestations of the underlying molecular structure involves simulations to identify system dynamics encoded in the spectroscopic signals, and requires computing the third-order polarization $P^{(3)}(t)$ [41, 101].

For linear spectroscopy, the autocorrelation function $F(t)$ can be calculate using the multi-$\mathrm{D}_2$ Ansatze as follows

$$F(t) = {}_{\text{ph}}\langle 0|_{\text{ex}}\langle 0|e^{iHt}Pe^{-iHt}P^{\dagger}|0\rangle_{\text{ex}}|0\rangle_{\text{ph}} = {}_{\text{ph}}\langle 0|_{\text{ex}}\langle 0|Pe^{-iHt}P^{\dagger}|0\rangle_{\text{ex}}|0\rangle_{\text{ph}}, \tag{25}$$

where $P = \mu\sum_n(|n\rangle_{\text{ex}}\,{}_{\text{ex}}\langle 0| + |0\rangle_{\text{ex}}\,{}_{\text{ex}}\langle n|)$. Fourier transformation of $F(t)$ leads to the linear absorption spectrum

$$\tilde{F}(\omega) = \frac{1}{\pi}\mathrm{Re}\int_0^{\infty} F(t)e^{i\omega t}dt. \tag{26}$$

It has been pointed out that $\tilde{F}(\omega)$ calculated using Davydov's Ansätze can help validate the Ansätze in parameter regimes of interest [37, 85, 86, 102].

In addition to linear spectra, multidimensional spectroscopic signals, such as two-dimensional (2D) photon echo (PE) spectra, yield elusive information on exciton scattering and dephasing in solids and solutions. Using the simulation of 2D PE spectra as an example, the interaction Hamiltonian is given by $\hat{H}_{\text{L}} = -\mathbf{E}(\mathbf{r},t)\cdot\hat{\mu}_{+} - \mathbf{E}^{*}(\mathbf{r},t)\cdot\hat{\mu}_{-}$, where $\mathbf{E}(r,t)$ is the electric field of the applied pulses,

$$\begin{aligned}
\mathbf{E}(\mathbf{r},t) &= \mathbf{E}_1(\mathbf{r},t) + \mathbf{E}_2(\mathbf{r},t) + \mathbf{E}_3(\mathbf{r},t),\\
\mathbf{E}_1(\mathbf{r},t) &= \mathbf{e}_1 E_1(t-\tau_1)\, e^{i\mathbf{k}_1\cdot\mathbf{r} - i\omega_1 t + i\phi_1},\\
\mathbf{E}_2(\mathbf{r},t) &= \mathbf{e}_2 E_2(t-\tau_2)\, e^{i\mathbf{k}_2\cdot\mathbf{r} - i\omega_2 t + i\phi_2},\\
\mathbf{E}_3(\mathbf{r},t) &= \mathbf{e}_3 E_3(t-\tau_3)\, e^{i\mathbf{k}_3\cdot\mathbf{r} - i\omega_3 t + i\phi_3},
\end{aligned} \tag{27}$$

where $\mathbf{e}_a$, $k_a$, $\omega_a$, $E_a(t)$, and $\phi_a$ $(a=1,2,3)$ denote the polarization, the wave vector, the frequency, the dimensionless envelope, and the initial phase, respectively [103, 104]. It is common to define the pulse arrival times in $\hat{H}_{\rm L}$ as $\tau_1=-T_w-\tau$, $\tau_2=-T_w$, $\tau_3=0$ where $\tau$ (the coherence time) is the delay time between the second and the first pulse, and $T_w$ (the population time) is the delay time between third and second pulse. In the short pulse limit, $E_a(t)=E_0\delta(t)$. It is assumed that the systems stays in $|g\rangle|0\rangle_{\rm ph}$ prior to the excitation ($t\ll -T-\tau$). Adopting the factorized initial condition allows for negligence of system-environment correlations. In the absence of excited-state absorption (ESA), the PE third polarization $P^{(3)}(t)$ consists of four response functions $R_{1-4}$, from which various 2D spectra can be computed [41, 103]. The third-order response is given by the response functions in the impulsive limit, which can be expressed in terms of the variational parameters of the Multi-$D_2$ Ansatz in Eq. (15) as follows [37, 104, 38, 74]

$$
\begin{aligned}
R_1(\tau,T_w,t) &= \sum_{i,j}^{M}\sum_{n,n_1,n_2,n_3}(\mathbf{e}_4^*\cdot\boldsymbol{\mu}_{n_2}^*)(\mathbf{e}_1\cdot\boldsymbol{\mu}_{n_3})(\mathbf{e}_2^*\cdot\boldsymbol{\mu}_n^*)(\mathbf{e}_3\cdot\boldsymbol{\mu}_{n_1})\\
&\quad\times A_{jn_1n}^*(T_w)A_{in_2n_3}(\tau+T_w+t)e^{\sum_q f_{jqn}^*(T_w)f_{iqn_3}(\tau+T_w+t)e^{i\omega_q t}}\\
&\quad\times e^{-\frac{1}{2}\sum_q(|f_{jqn}(T_w)|^2+|f_{iqn_3}(\tau+T_w+t)|^2)},\\
R_2(\tau,T_w,t) &= \sum_{i,j}^{M}\sum_{n,n_1,n_2,n_3}(\mathbf{e}_4^*\cdot\boldsymbol{\mu}_{n_2}^*)(\mathbf{e}_1^*\cdot\boldsymbol{\mu}_n^*)(\mathbf{e}_2\cdot\boldsymbol{\mu}_{n_3})(\mathbf{e}_3\cdot\boldsymbol{\mu}_{n_1})\\
&\quad\times A_{jn_1n}^*(\tau+T_w)A_{in_2n_3}(T_w+t)e^{\sum_q f_{jqn}^*(\tau+T_w)f_{iqn_3}(T_w+t)e^{i\omega_q t}}\\
&\quad\times e^{-\frac{1}{2}\sum_q(|f_{jqn}(\tau+T_w)|^2+|f_{iqn_3}(T_w+t)|^2)},\\
R_3(\tau,T_w,t) &= \sum_{i,j}^{M}\sum_{n,n_1,n_2,n_3}(\mathbf{e}_4^*\cdot\boldsymbol{\mu}_{n_2}^*)(\mathbf{e}_1^*\cdot\boldsymbol{\mu}_n^*)(\mathbf{e}_2\cdot\boldsymbol{\mu}_{n_1})(\mathbf{e}_3\cdot\boldsymbol{\mu}_{n_3})\\
&\quad\times A_{jn_1n}^*(\tau)A_{in_2n_3}(t)e^{\sum_q f_{jqn}^*(\tau)f_{iqn_3}(t)e^{i\omega_q(T_w+t)}}\\
&\quad\times e^{-\frac{1}{2}\sum_q(|f_{jqn}(\tau)|^2+|f_{iqn_3}(t)|^2)},\\
R_4(\tau,T_w,t) &= \sum_{i,j}^{M}\sum_{n,n_1,n_2,n_3}(\mathbf{e}_4^*\cdot\boldsymbol{\mu}_n^*)(\mathbf{e}_1^*\cdot\boldsymbol{\mu}_{n_3}^*)(\mathbf{e}_2\cdot\boldsymbol{\mu}_{n_2})(\mathbf{e}_3\cdot\boldsymbol{\mu}_{n_1})\\
&\quad\times A_{jn_1n}^*(-t)A_{in_2n_3}(\tau)e^{\sum_q f_{jqn}^*(-t)f_{iqn_3}(\tau)e^{-i\omega_q T_w}}\\
&\quad\times e^{-\frac{1}{2}\sum_q(|f_{jqn}(-t)|^2+|f_{iqn_3}(\tau)|^2)}.
\end{aligned}
\tag{28}
$$

Here $\boldsymbol{\mu}_n$ are the transition dipole moments, and $\mathbf{e}_4$ is the polarization of the local oscillator field. $A_{jn_1n}^*(t)$ is the exciton amplitude at state $|n_1\rangle$ of the $j$th Gaussian superposition and with respect to initial state $|n\rangle$, and $f_{jqn}(t)$ is the corresponding phonon deformations with respect to $|n\rangle\exp\left\{\sum_q^{N_q}\left[f_{jq}(0)\hat{b}_q^\dagger-f_{jq}^*(0)\hat{b}_q\right]\right\}|\mathbf{0}\rangle_{\rm ph}$.

Correspondingly, one obtains the higher excited-state response functions [104, 105]

$$
\begin{aligned}
R_1^*(\tau,T_w,t) &= \sum_{i,j}^{M}\sum_{\substack{nn_1n_2\\ n_3m}} (\mathbf{e}_4^*\cdot\boldsymbol{\mu}_{n_1m}^*)(\mathbf{e}_1^*\cdot\boldsymbol{\mu}_n^*)(\mathbf{e}_2\cdot\boldsymbol{\mu}_{n_3})(\mathbf{e}_3\cdot\boldsymbol{\mu}_{n_2m}) \\
&\quad A^{j*}_{m(n_1n)}(0)A^{i}_{m(n_2n_3)}(t)e^{\sum_q f^{j*}_{m(n_1n),q}(0)f^{i}_{m(n_2n_3),q}(t)}e^{-\frac{1}{2}\sum_q(|f^{j*}_{m(n_1n),q}(0)|^2+|f^{i}_{m(n_2n_3),q}(t)|^2)}, \\
R_2^*(\tau,T_w,t) &= \sum_{i,j}^{M}\sum_{\substack{nn_1n_2\\ n_3m}} (\mathbf{e}_4^*\cdot\boldsymbol{\mu}_{n_1m}^*)(\mathbf{e}_1\cdot\boldsymbol{\mu}_{n_3})(\mathbf{e}_2^*\cdot\boldsymbol{\mu}_n^*)(\mathbf{e}_3\cdot\boldsymbol{\mu}_{n_2m}) \\
&\quad A^{j'*}_{m(n_1n)}(0)A^{i'}_{m(n_2n_3)}(t)e^{\sum_q f^{j'*}_{m(n_1n),q}(0)f^{i'}_{m(n_2n_3),q}(t)}e^{-\frac{1}{2}\sum_q(|f^{j'*}_{m(n_1n),q}(0)|^2+|f^{i'}_{m(n_2n_3),q}(t)|^2)}.
\end{aligned}
$$

The initial amplitudes of the higher excited-state are $A^{j*}_{m(n_1n)}(0)=A^*_{jn_1n}(\tau+T_w+t)$, $A^{i}_{m(n_2n_3)}(0)=A_{in_2n_3}(T_w)$, $A^{j'*}_{m(n_1n)}(0)=A^*_{jn_1n}(t+T_w)$, and $A^{i'}_{m(n_2n_3)}(0)=A_{in_2n_3}(\tau+T_w)$, and the corresponding phonon deformations are $f^{j*}_{m(n_1n),q}(0)=f^*_{jn_1q}(\tau+T_w+t)$, $f^{i}_{m(n_2n_3),q}(0)=f_{in_2q}(T_w)$, $f^{j'*}_{m(n_1n),q}(0)=f^*_{jn_1q}(t+T_w)$, and $f^{i'}_{f(n_2n_3),q}(0)=f_{in_2q}(\tau+T_w)$.

Consequently, one arrives at the stimulated emission (SE), the ground-state bleach (GSB), and the ESA contributions, respectively, [41, 103]

$$
\begin{aligned}
S_{\rm SE}(\omega_\tau,T_w,\omega_t) &= \Re\int_0^\infty\int_0^\infty dtd\tau[R_1(\tau,T_w,t)e^{-i\omega_\tau\tau+i\omega_t t}+R_2(\tau,T_w,t)e^{i\omega_\tau\tau+i\omega_t t}], \\
S_{\rm GSB}(\omega_\tau,T_w,\omega_t) &= \Re\int_0^\infty\int_0^\infty dtd\tau[R_3(\tau,T_w,t)e^{-i\omega_\tau\tau+i\omega_t t}+R_4(\tau,T_w,t)e^{i\omega_\tau\tau+i\omega_t t}], \\
S_{\rm ESA}(\omega_\tau,T_w,\omega_t) &= -\Re\int_0^\infty\int_0^\infty dtd\tau[R_1^*(\tau,T_w,t)e^{-i\omega_\tau\tau+i\omega_t t}+R_2^*(\tau,T_w,t)e^{i\omega_\tau\tau+i\omega_t t}]. \quad (29)
\end{aligned}
$$

The sum of the above three contributions delivers the correlated 2D spectrum

$$
S(\omega_\tau,T_w,\omega_t)=S_{\rm SE}(\omega_\tau,T_w,\omega_t)+S_{\rm GSB}(\omega_\tau,T_w,\omega_t)+S_{\rm ESA}(\omega_\tau,T_w,\omega_t). \quad (30)
$$

# 5 Variational dynamics at finite temperatures

## 5.1 Monte Carlo importance sampling

In Sec. 3, we only explained the zero-temperature time-dependent variation. However, a majority of measurements are conducted at finite temperatures, so it is important to also simulate many-body quantum dynamics and corresponding spectral signatures at finite temperatures. To generalize the variational approach to finite temperatures, we will use a Monte Carlo procedure analogous to the one employed in ML-MCTDH in this section [55, 71].

To illustrate the finite-temperature approach, $\hat{H}_{\rm SBM}$ of Eq. (10) is used here as an example. The initial system density matrix is assumed to be factorized, *i.e.*, $\hat{\rho}_{\rm tot}(0)=\hat{\rho}(0)\hat{\rho}_{\rm B}^{\rm eq}$, where $\hat{\rho}(0)=|+\rangle\langle+|$.

It is straightforward to extend the description to more general initial conditions with superpositions of $|-\rangle$ and $|+\rangle$. We proceed to calculate the the expectation value of an observable $\hat{O}(t)$

$$\langle\hat{O}(t)\rangle = \mathrm{Tr}\{\hat{O}e^{-i\hat{H}_{\mathrm{SBM}}t}\hat{\rho}_{\mathrm{B}}^{\mathrm{eq}}|1\rangle\langle 1|e^{i\hat{H}_{\mathrm{SBM}}t}\}. \tag{31}$$

The coherent state representation is used for the task,

$$\langle\hat{O}(t)\rangle = \pi^{-N_b}\int d^2\boldsymbol{\alpha}\langle\boldsymbol{\alpha}|\langle 1|\hat{\rho}_{\mathrm{B}}^{\mathrm{eq}}e^{i\hat{H}_{\mathrm{SBM}}t}\hat{O}e^{-i\hat{H}_{\mathrm{SBM}}t}|1\rangle|\boldsymbol{\alpha}\rangle. \tag{32}$$

$|\boldsymbol{\alpha}\rangle = \exp(\sum_l \alpha_l b_l^\dagger - \mathrm{H.c.})\big|0\big\rangle_{\mathrm{B}}$, where the sum in the exponent is over all $N_b$ bath modes. The bath equilibrium density matrix can be written as [93, 106]

$$\hat{\rho}_{\mathrm{B}}^{\mathrm{eq}} = \int d^2\boldsymbol{\alpha}\, p(\boldsymbol{\alpha};\,\beta)|\boldsymbol{\alpha}\rangle\langle\boldsymbol{\alpha}|, \tag{33}$$

where $\beta = 1/(k_B T)$, and $p(\boldsymbol{\alpha};\,\beta)$ denotes the diagonal elements in coherent-state representation, [107]

$$p(\boldsymbol{\alpha};\,\beta) = \prod_l^{N_b}\left[\frac{e^{\beta\omega_l}-1}{\pi}\exp\left(-|\alpha_l|^2(e^{\beta\omega_l}-1)\right)\right]. \tag{34}$$

Seen as a probability density, $p(\boldsymbol{\alpha};\,\beta)$ is a positive-definite function of $\boldsymbol{\alpha}$ as shown in Eq. (34). Substituting Eq. (33) into Eq. (32), the finite-temperature observables $\langle\hat{O}(t)\rangle$ are evaluated by the average according to the probability density $p(\boldsymbol{\alpha};\,\beta)$ as

$$\begin{aligned}\langle\hat{O}(t)\rangle &= \int d^2\boldsymbol{\alpha}p(\boldsymbol{\alpha};\,\beta)\langle\boldsymbol{\alpha}|\langle 1|e^{i\hat{H}_{\mathrm{SBM}}t}\hat{O}e^{-i\hat{H}_{\mathrm{SBM}}t}|1\rangle|\boldsymbol{\alpha}\rangle \\ &= \int d^2\boldsymbol{\alpha}p(\boldsymbol{\alpha};\,\beta)\langle \mathrm{D}_{1,2}^M(t;\,\boldsymbol{\alpha})|\hat{O}|\mathrm{D}_{1,2}^M(t;\,\boldsymbol{\alpha})\rangle,\end{aligned} \tag{35}$$

where we have used substitution $\big|\mathrm{D}_{1,2}^M(t;\,\boldsymbol{\alpha})\big\rangle = e^{-i\hat{H}_{\mathrm{SBM}}t}\big|1\big\rangle\big|\boldsymbol{\alpha}\big\rangle$, and $\big|\mathrm{D}_{1,2}^M(0;\,\boldsymbol{\alpha})\big\rangle = \big|1\big\rangle\big|\boldsymbol{\alpha}\big\rangle$ is a trial state with bath displacements of $\boldsymbol{\alpha}$ at $t=0$. For the multi-$\mathrm{D}_1$ Ansatz, initial parameters are $A_1(0)=1$, $B_1(0)=0$, $A_n(0)=B_n(0)=0$ for $n\neq 1$ and $f_{nl}(0)=g_{nl}(0)=\alpha_l$ for all $n$ and $l$; and for the multi-$\mathrm{D}_2$ Ansatz, $A_1(0)=1$, $B_1(0)=0$, $A_n(0)=B_n(0)=0$ for $n\neq 1$ and $f_{nl}(0)=\alpha_l$ for all $n$ and $l$. Any observable expectation value can be calculated via Monte Carlo importance sampling as

$$\langle\hat{O}(t)\rangle = \frac{1}{N_s}\sum_i^{N_s}\langle \mathrm{D}_{1,2}^M(t;\,\boldsymbol{\alpha}_i)|\hat{O}|\mathrm{D}_{1,2}^M(t;\,\boldsymbol{\alpha}_i)\rangle, \tag{36}$$

where $N_s$ is the sampling number. The bath configuration $\boldsymbol{\alpha}_i$ is generated according to $p(\boldsymbol{\alpha};\,\beta)$ by importance sampling. Given $2\sigma_l^2 = 1/(e^{\beta\omega_l}-1)$ and $\alpha_l = x_l + ip_l$, one may partition $p(\boldsymbol{\alpha};\,\beta)$ in Eq. (34) into two independent Gaussian distributions with $\sigma_l$ as their variance,

$$p(\boldsymbol{\alpha};\,\beta) = \prod_l^{N_b}\frac{1}{\sqrt{2\pi}\sigma_l}e^{-\frac{x_l^2}{2\sigma_l^2}}\frac{1}{\sqrt{2\pi}\sigma_l}e^{-\frac{p_l^2}{2\sigma_l^2}}. \tag{37}$$

To bypass numerical singularities, boson displacements are initialized by setting $f_{nl}(0) = g_{nl}(0) = \alpha_l + \epsilon_0$ with noise $\epsilon_0$ obeying the uniform distribution $[-10^{-2}, 10^{-2}]$. The zero temperature case corresponds to $\alpha_l = 0$ for all $l$, and the observable of Eq. (36) is reduced to $\langle \mathrm{D}_{1,2}^M(t)|\hat{O}|\mathrm{D}_{1,2}^M(t)\rangle$.

### 5.2 Displaced number states

Another way of including temperature effects with the HDA methodology is to use displaced number states, as initialization of the bath degrees of freedom (DOFs) may be readily captured by displaced number states. It is shown that the method of displaced number states with the multi-$\mathrm{D}_2$ Ansatz delivers accurate, efficient descriptions of nonadiabatic dynamics at conical intersections (CIs) [74]. The multi-$\mathrm{D}_2$ trial state of multiplicity $M$ for the displaced number state is given by [73, 74]

$$|\mathrm{D}_2^{\vec{n},M}(t)\rangle = \sum_m |m\rangle \sum_{k=1}^M A_{m,k}^{\vec{n}}(t) e^{\left(\sum_q f_{kq}^{\vec{n}}(t) b_q^\dagger - H.c.\right)} |\vec{n}\rangle,$$

where $|\vec{n}\rangle = |n_1 n_2 \cdots n_w\rangle$, and $|m\rangle$ are the diabatic states. Variational parameters $\vec{\mu} = \{A_{mk}^{\vec{n}}(t), f_{kq}^{n_q}(t)\}$ are obtained from the usual time-dependent variation after constructing the Lagrangian. A quick way to move forward is to expand initially excited number states in terms of coherent states, then to obtain the standard EOMs but with nontrivial initial conditions to be sampled along a phase-space circle. This approach greatly speeds up the numerics, and will be described below in detail.

The number state $|n_l\rangle$ may be express by superpositions of coherent states [73],

$$|n_l\rangle = \frac{1}{2\pi} \sqrt{\frac{n_l! e^{|\beta_l|^2}}{|\beta_l|^{2n_l}}} \int_{-\pi}^{\pi} d\theta_l e^{-in_l\theta_l} ||\beta_l| e^{i\theta_l}\rangle. \tag{38}$$

To discretize the integral over $\theta_l$, an approximate expression can be adopted as below

$$|n_l\rangle \approx \sqrt{\frac{n_l! e^{|\beta_l|^2}}{|\beta_l|^{2n_l}}} \frac{1}{N} \sum_{k_l=0}^{N-1} e^{-in_l\theta_{k_l}} ||\beta_l| e^{i\theta_{k_l}}\rangle, \tag{39}$$

where $\theta_{k_l} = -\pi + \frac{2\pi}{N} k_l$ and $k_l = 0, ..., N-1$. For the multi-$\mathrm{D}_2$ Ansatz with multiplicity $M \geq N^w$ ($w$ being the number of modes excited), variational parameters with $w$ phonon modes can be initialized as [73]

$$A_{m,k}^{\vec{n}}(0) = \begin{cases} \prod_l \mathcal{N}(\beta_l) \exp(-in_l\theta_{k_l}), & 1 \leq k \leq N^w. \\ 0, & \text{else.} \end{cases} \tag{40}$$

$$A_{m',k}^{\vec{n}}(0) = 0, (\text{for } \ m' \neq m). \tag{41}$$

$$f_{kl}^{n_l}(0) = \begin{cases} |\beta_l| \exp(i\theta_{k_l}), & 1 \leq k \leq N^w. \\ 0, & \text{else,} \end{cases} \tag{42}$$

where $\mathcal{N}(\beta_l) = \frac{1}{N}\sqrt{\frac{(n_l!)e^{\beta_l^2}}{|\beta_l|^{2n_l}}}$. Quick convergence with respect to the number of sampling points $N$ on a circle of radius $|\beta_l| = \sqrt{n_l}$ can be obtained, for instance, for $N$ between 5 and 14 depending on initial excitations $n$ (see Ref. [96]). The best performance value of $|\beta_l| = \sqrt{n_l}$ is often adopted. Population of the diabatic state $|m\rangle$ for the number state $|\vec{n}\rangle$ takes the form

$$P_m^{\vec{n}} = \sum_k^M \sum_{k'}^M A_{m,k}^{\vec{n}*}(t) A_{m,k'}^{\vec{n}}(t) S_{kk'}^{\vec{n}},$$

where

$$S_{kk'}^{\vec{n}} = \exp\left(\sum_q \left\{ -\left(\left|f_{kq}^{n_q}\right|^2 + \left|f_{k'q}^{n_q}\right|^2\right)/2 + f_{kq}^{n_q *} f_{k'q}^{n_q} \right\}\right). \tag{43}$$

Thermal averaging can be implemented as follows

$$P_m^B = \prod_l \sum_{n_l=0}^{N_{l,T}} \frac{e^{-\beta n_l \omega_l}}{Q_\beta} P_m^{\vec{n}},$$

where the partition function is given by

$$Q_\beta = \prod_l \sum_{n_l=0}^{\infty} e^{-\beta n_l \omega_l}. \tag{44}$$

The truncation number of the $l$th mode excitation, $N_{l,T}$, which ensures numerical convergence, is jointly determined by the total phonon excitation energy and the temperature.

### 5.3 Thermofield dynamics

The TFD approach was proposed in the 1970s as a wave-function based formalism of quantum dynamics at finite temperatures [108, 109, 110, 76]. It has recently emerged to be a powerful tool for finite-temperature description of many-body quantum dynamics when used in combination with highly efficient numerical integration schemes of multidimensional quantum dynamics such as the HDA methodology [79] or the tensor-train approach [111, 112, 113]. The TFD approach can be readily applied to the vibronic coupling (VC) Hamiltonians, such as the Hamiltonians of Eqs. (1) and (10), in which diabatic potential energy surfaces (PESs) are given by polynomials of nuclear coordinates [114, 115, 116, 117, 118, 119] To give a concise introduction to the TFD method, the finite-temperature SBM will be used as an example and the presentation of Sec. 5.1 will be followed. The SBM dynamics is represented by the density matrix $\hat{\rho}_{\rm tot}(t)$ which follows the Liouville-von Neumann equation

$$\partial_t \hat{\rho}_{\rm tot}(t) = -i[\hat{H}_{\rm SBM}, \hat{\rho}_{\rm tot}(t)], \;\; \hat{\rho}_{\rm tot}(0) = |+\rangle\langle +| \hat{\rho}_{\rm B}^{\rm eq}. \tag{45}$$

Following Ref. [120], the bath-manifold eigenstates are introduced, $\hat{H}_{\rm B}|\boldsymbol{k}\rangle = E_{\boldsymbol{k}}|\boldsymbol{k}\rangle$. Apparently, $|\boldsymbol{k}\rangle = \prod_l |k_l\rangle$ where $E_{\boldsymbol{k}} = \sum_l k_l\omega_l$ and $|k_l\rangle$ are the $l$th-mode eigenstates. Vectors $|\tilde{\boldsymbol{k}}\rangle$ are a copy of $|\boldsymbol{k}\rangle$ in the so-called *tilde* Hilbert space. With the notation $|\boldsymbol{k}\tilde{\boldsymbol{k}}\rangle = |\boldsymbol{k}\rangle|\tilde{\boldsymbol{k}}\rangle$, one may define the unity vector $|\boldsymbol{I}\rangle = \sum_{\boldsymbol{k}} |\boldsymbol{k}\tilde{\boldsymbol{k}}\rangle$ and the thermal vacuum state,

$$|\mathbf{0}(\beta)\rangle = \sqrt{\hat{\rho}_{\rm B}^{\rm eq}}|\boldsymbol{I}\rangle = Z_{\rm B}^{-\frac{1}{2}} e^{-\frac{1}{2}\hat{H}_{\rm B}}|\boldsymbol{I}\rangle, \tag{46}$$

where $Z_{\rm B}$ is the partition function. It follows that the Boltzmann distribution takes the form of $\hat{\rho}_{\rm B}^{\rm eq} = {\rm Tr}_{\tilde{\boldsymbol{k}}}\{|\mathbf{0}(\beta)\rangle\langle\mathbf{0}(\beta)|\}$, where ${\rm Tr}_{\tilde{\boldsymbol{k}}}\{...\}$ denotes a trace over the tilde subspace. The Liouvill-von Neumann equation reads

$$\partial_t\hat{\sigma}_{\rm tot}(t) = -i[\hat{H}_{\rm SBM}, \hat{\sigma}_{\rm tot}(t)],\ \ \hat{\sigma}_{\rm tot}(0) = |+\rangle\langle+||\mathbf{0}(\beta)\rangle\langle\mathbf{0}(\beta)|. \tag{47}$$

Obviously, $\hat{\rho}_{\rm tot}(t) = {\rm Tr}_{\tilde{\boldsymbol{k}}}\{\hat{\sigma}_{\rm tot}(t)\}$. Furthermore, Eq. (45) in which $\hat{H}_{\rm SBM} \to \hat{H}_{\rm SBM} - \tilde{h}$ ($\tilde{h}$ being any operator acting in the tilde subspace) produces $\hat{\sigma}_{\rm tot}(t)$ which yields the same $\hat{\rho}_{\rm tot}(t)$. Since the initialization of Eq. (47) corresponds to a pure state, one has

$$\hat{\sigma}_{\rm tot}(t) = |\psi(t)\rangle\langle\psi(t)| \tag{48}$$

where $|\psi(t)\rangle$ is governed by the TFD Schrödinger equation

$$\partial_t|\psi(t)\rangle = -i(\hat{H}_{\rm SBM} - \tilde{h})|\psi(t)\rangle,\ \ |\psi(0)\rangle = |+\rangle|\mathbf{0}(\beta)\rangle. \tag{49}$$

Therefore, the solution to the original Liouville-von Neumann equation (45) has been shown to be equivalent to that to the TFD Schrödinger equation (49).

The TFD approach has the key advantage of having a compact analytical expression for the thermal vacuum state thanks to the Bogoliubov transformation

$$e^{-iG}|\mathbf{0}\tilde{\mathbf{0}}\rangle = |\mathbf{0}(\beta)\rangle \tag{50}$$

where $|\mathbf{0}\tilde{\mathbf{0}}\rangle$ is the ground state in the $|\boldsymbol{k}\rangle \otimes |\tilde{\boldsymbol{k}}\rangle$ subspace. After the application of the Bogoliubov transformation to Eq. (49), one has

$$i\partial_t|\psi_\theta(t)\rangle = \hat{H}_{\rm SBM}^{\theta}|\psi_\theta(t)\rangle,\ \ |\psi_\theta(0)\rangle = |+\rangle|\mathbf{0}\tilde{\mathbf{0}}\rangle \tag{51}$$

where $\hat{H}_{\rm SBM}^{\theta} = e^{iG}(\hat{H}_{\rm SBM} - \tilde{h}_v)e^{-iG}$, $|\psi_\theta(t)\rangle = e^{iG}|\psi(t)\rangle$. For thermal vacuum state $|\mathbf{0}(\beta)\rangle$ of Eq. (46), the Bogoliubov transformation takes the form of $G = -i\sum_l \theta_l(b_l\tilde{b}_l - b_l^\dagger\tilde{b}_l^\dagger)$ with $\theta_l = {\rm arctanh}(e^{-\beta\omega_l/2})$ [76, 108, 109, 110]. To get an explicit form of the transformed Hamiltonian $\hat{H}_{\rm SBM}^{\theta}$, we choose $\tilde{h} =$

$\sum_l \omega_l \tilde{b}_l^\dagger \tilde{b}_l$ [113], leading to the TFD Schrödinger equation (51) in which [113]

$$\begin{aligned}
\hat{H}^\theta_{\rm SBM} &= \hat{H}^\theta_{\rm S} + \hat{H}^\theta_{\rm SB} + \hat{H}^\theta_{\rm B}, \\
\hat{H}^\theta_{\rm S} &= \hat{H}_{\rm S}, \\
\hat{H}^\theta_{\rm SB} &= \frac{\sigma_z}{2} \sum_l \lambda_l \left[ \cosh(\theta_l)(b_l^\dagger + b_l) + \sinh(\theta_l)(\tilde{b}_l^\dagger + \tilde{b}_l) \right], \\
\hat{H}^\theta_{\rm B} &= \sum_l \omega_l \left[ b_l^\dagger b_l - \tilde{b}_l^\dagger \tilde{b}_l \right].
\end{aligned} \tag{52}$$

The TFD Schrödinger equation (51) with $\hat{H}^\theta_{\rm SBM}$ of Eq. (52) is equivalent to the Liouville-von Neumann equation (45) with $\hat{H}_{\rm SBM}$, and all observables evaluated via Eqs. (51) and (45) are identical. The total phonon-mode number in $\hat{H}^\theta_{\rm SBM}$ doubles that in $\hat{H}_{\rm SBM}$ of Eq. (10), and electron-phonon coupling strengths in $\hat{H}^\theta_{\rm SBM}$ are renormalized by temperature-dependent factors: $\cosh(\theta_l)$ for the physical modes and $\sinh(\theta_l)$ for the tilde modes. If $T \to 0$, then $\theta_l \to 0$, with vanishing coupling to the tilde space, and the standard Schrödinger equation fully reinstated. Temperature effects enter the system via dynamically mingling the physical ($b_l$, $b_l^\dagger$) and the tilde ($\tilde{b}_l$, $\tilde{b}_l^\dagger$) variables. It is essential that the TFD Hamiltonian of Eq. (52) is isomorphic with the original SBM Hamiltonian of Eq. (10). The TFD Schrödinger equation (51) can be treated as the usual Schrödinger equation, with all relevant derivations unaffected.

# 6 The spin-boson model and its variants

Popularized by Leggett, the SBM is a paradigmatic instrument for the study of a two-state system interacting with a dissipative bath [121]. We summarize in this section a few recent applications of Davydov's Ansätze to the ground-state and the dynamic properties of the SBM variants, including the sinusoidally driven SBM, the two-bath SBM, the two-spin SBM, and the cavity-embedded SBM.

Despite much theoretical and numerical work devoted to the SBM, a consensus remains elusive on the dynamics of Hamiltonian (10) in much of the phase diagram. Shown in Fig. 2 is a rough sketch of the dynamics phase diagram of SBM obtained using the multi-$D_1$ Ansatz with Monte Carlo importance sampling (as discussed in Sec. 5.1). The spectral density form $J(\omega) = 2\alpha\omega_c^{1-s}\omega^s e^{-\omega/\omega_c}$ is adopted, where $\omega_c$ is the cutoff frequency, $\alpha$ is the coupling strength, and $s$ is the spectral exponent. We set $\epsilon = 0$ and $\Delta = \omega_c/10$.. It is believed that for $s \leq 1$, with increasing coupling strength $\alpha$, a dynamical coherent-incoherent crossover occurs before a delocalized-to-localized transition, as unveiled by an ML-MCTDH approach and the technique of quantum master equations [122, 123, 124, 125]. As shown in Fig. 2, the solid line separates the localized phase (upper) from the delocalized phase (lower), while two dashed lines meet at the critical point $s_c$ marking the coherent-incoherent

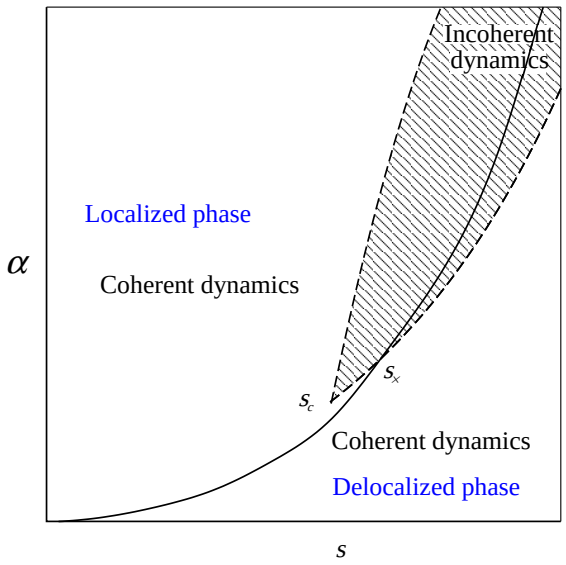


Figure 2: A rough drewing of the SBM phase diagram. The solid line separates the delocalized phase (lower) from the localized phase (upper), while the dashed lines mark the coherent-incoherent crossover. The lower dashed line intersects with the solid line at $s_\times$, and the two dashed lines meet at the critical point $s_c$. For $s_c < s < 1$, the two dashed lines map the domain into three parts with shaded area corresponding to the incoherent state. Outside the shaded area is the coherent state. For $s < s_c$, there is only the coherent state. We set $\epsilon = 0$ and $\Delta = \omega_c/10$.

crossover. The lower dashed line intersects with the solid line at $s_\times$. The shaded area bordered by the dashed lines in Fig. 2 represents the incoherent phase, and the rest of the phase diagram is the coherent phase. The solid line in Fig. 2 depicts the localized-delocalized phase transition and intersects with the coherent-incoherent transition line at $s_\times$, which is larger than $s_c$. For the sub-Ohmic dephasing fluctuations case, a similar phase diagram can be obtained [126]. Most recent results from the numerically "exact" QUAPI method seem to lend support and explanation to the topology of such phase diagrams [127], while an additional study using the multi-$D_1$ Ansatz reveals substantial effects of the system and bath initialization on the dynamic phase diagram [128].

As shown in the upper panel of Fig. 3, the low-temperature dynamics ($k_B T/\omega_c = 0.01$) from the $D_1^{M=2}$ Ansatz and QUAPI are in perfect agreement. At high temperatures ($k_B T/\omega_c = 0.2$), dynamics obtained by the $D_1^{M=2}$ Ansatz and QUAPI remain in good agreement despite a tiny discrepancy between the QUAPI and the $D_1^{M=2}$ Ansatz populations, which may be attributed to insufficient number of bath modes in the variational method, as displayed in the lower panel of Fig. 3. From Eq. (37), $\sigma_l$ inflates at high temperatures, leading to large values of $f_{nl}(0)$ and $g_{nl}(0)$ for high-frequency modes which may be safely disregarded at low temperatures. It follows that the required modes number $N_b$ of and the sampling number increase at high temperatures. However, the single

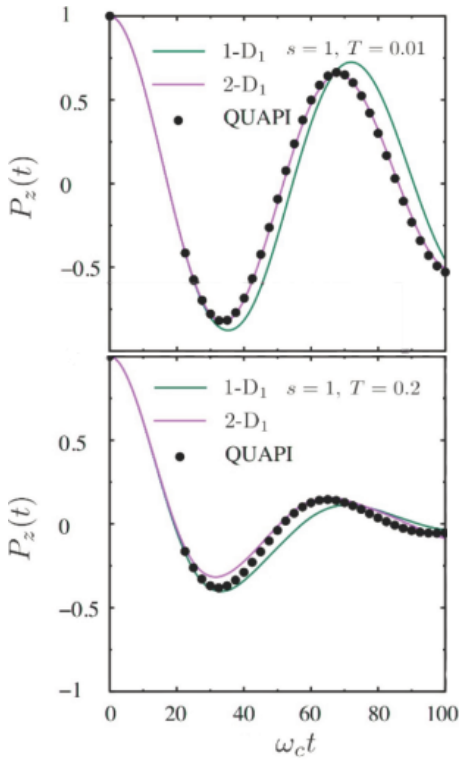


Figure 3: Population difference $P_z(t)$ comnputed by the multi-$D_1$ Ansätze (solid lines) with $M = 1$ (1-$D_1$, green) and $M = 2$ (2-$D_1$, purple) and the QUAPI approach (black circles) for $s = 1$, $\epsilon = 0$, $\Delta$=0.1, $\alpha = 0.05$, and two temperatures, $T/\omega_c = 0.01$ and 0.2. The initial condition of a factorized bath is used.

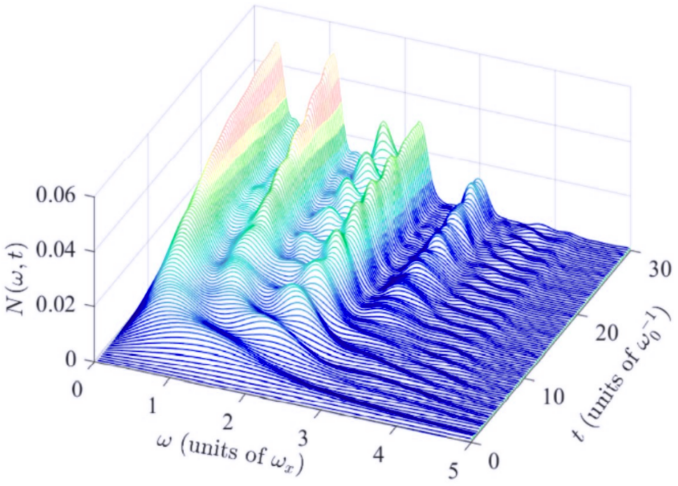


Figure 4: Time-dependent fluorescence plotted as a function of frequency $\omega$ and time $t$ from the multi-$D_1$ Ansatz for $\alpha = 0.1$, $\omega_0 = 0.2\omega_c$, $\omega_x = \omega_0$, and $\Omega = 1.5\omega_0$ with $N_b = 150$ and $M = 15$.

$D_2$ Ansatz ($M = 1$)is considerably more accurate at high temperatures than at low temperatures (cf. the upper panel of Fig. 3). As a result, the increased CPU time due to the added bath modes and increased sampling is compensated by a reduced Ansatz multiplicity, so the Davydov-Ansatz method with importance sampling remains efficient at high temperatures.

### 6.1 The driven spin-boson model

The multi-$D_1$ Ansatz has also been applied to a sinusoidally driven SBM problem [97]:

$$H(t) = \frac{1}{2}\omega_0\sigma_z + \Omega\cos(\omega_x t)\sigma_x + H_{\rm R} + H_{\rm SR}, \tag{53}$$

where $\omega_0$ is the qubit transition frequency and $\sigma_{z,x}$ are the Pauli matrices. $\Omega$ is the Rabi frequency and $\omega_x$ is the driving frequency. $H_{\rm R} = \sum_{k=1}^{N_b}\omega_k b_k^\dagger b_k$, with $b_k$ ($b_k^\dagger$) the annihilation (creation) operator of the $k$th bosonic mode and $N_b$ the mode number. The qubit-reservoir coupling Hamiltonoian $H_{\rm SR}$ reads $H_{\rm SR} = \sigma_x/2\sum_{k=1}^{N_b}\lambda_k(b_k + b_k^\dagger)$, where $\lambda_k$ is the coupling strength between the $k$th mode and qubit, giving rise to an Ohmic spectral density $J(\omega) = \sum_{k=1}^{N_b}\lambda_k^2\delta(\omega-\omega_k) = 2\alpha\omega\Theta(\omega_c-\omega)$, where $\alpha$ is a dimensionless coupling strength, $\omega_c$ is the cut-off frequency, and $\Theta(\cdot)$ is the Heaviside step function. Time evolution of the bosonic population can be computed for each bath mode by using the multi-$D_1$ Ansatz, and consequently, the time-resolved fluorescence spectrum can be evaluated accurately. Fig. 4 shows the photon number distribution versus emission frequency and time, which unveils the real-time formation of emission peaks [97]. The variational method with the multi-$D_1$ Ansatz offers a powerful tool to compute the spectral evolution, capturing accurate dynamics of both the qubit and the field.

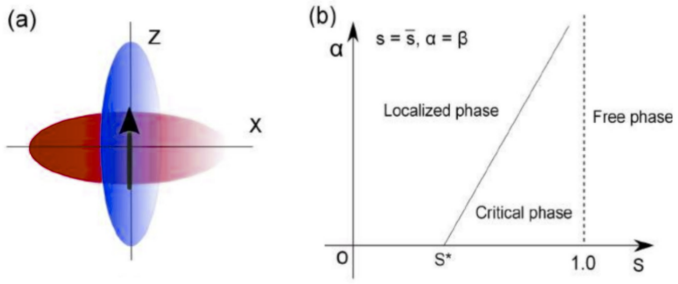


Figure 5: (a) Schematic of a 2-bath SBM. One spin is coupled to two independent baths with diagonal (Z) or off-diagonal (X) spin-bath coupling. (b) Schematic plot of the phase diagram of the 2-bath SBM with two identical baths $s = \bar{s}$ and $\alpha = \beta$, where $s$ ($\bar{s}$) and $\alpha$ ($\beta$) represent the spectral exponents and coupling strengths, respectively, for the bath spectral density functions $J_z(\omega)$ ($J_x(\omega)$). Three phases (localized, critical and free) are displayed in the $s$-$\alpha$ plane with two critical spectral exponent values, $s^*$ and 1.0.

### 6.2 The two-bath spin-boson model

There are several studies extending the standard SBM. One way is to couple the spin to a bath with simultaneous diagonal and off-diagonal coupling [129]. Another way is to couple a single spin to two baths, each with its individual form of spin-bath coupling. It is handy to use the multi-$D_1$ Ansatz to investigate a two-bath SBM which is given by

$$\hat{H}_{\rm SBM}^{2-{\rm bath}} = \frac{\varepsilon}{2}\sigma_z - \frac{\Delta}{2}\sigma_x + \sum_{l,i}\omega_l b_{l,i}^\dagger b_{l,i} + \frac{\sigma_z}{2}\sum_l \lambda_l (b_{l,1}^\dagger + b_{l,1}) + \frac{\sigma_x}{2}\sum_l \phi_l (b_{l,2}^\dagger + b_{l,2}), \tag{54}$$

where $i = 1, 2$ is the bath index, $\lambda_l$ ($\phi_l$) is the diagonal (off-diagonal) coupling strength for the $l$th bath mode, and $\varepsilon$ and $\Delta$ are the spin bias and tunneling constant, respectively. To study quantum phase transitions (QPTs), we set $\varepsilon = \Delta = 0$ and adopt a logarithmic discretization scheme by partitioning the frequency domain $[0, \omega_c]$ into $L$ intervals $\omega_c[\Lambda^{-l}, \Lambda^{-(l-1)}]$, where $l = 1, 2, \ldots, L$, and we set $\omega_c = 1$ and $\Lambda = 2$ [130].

The 2-bath SBM of Eq. (54) has been recently examined using the HDA methodology [35, 131, 132], yielding a phase diagram as displayed in Fig. 5(b). The arrow in Fig. 5(a) denotes a spin, and Z and X refer to the diagonal and off-diagonal coupling, respectively, with corresponding bath spectral densities given by $J_z(\omega) = 2\alpha\omega_c^{1-s}\omega^s$ and $J_x(\omega) = 2\beta\omega_c^{1-\bar{s}}\omega^{\bar{s}}$. Here $\alpha$ and $\beta$ are the dimensionless coupling strengths, and $s$ and $\bar{s}$ denote the spectral exponents. The 2-bath SBM may be realized in the lab as an impurity in a magnet coupled to two spin-wave modes [133, 134, 135, 136], a superconducting qubit connected to electromagnetic fluctuations of two linear circuits, [137, 138, 139], a SQUID-based charge qubit coupled to two cavity fields[140], and thermal transport between two reservoirs coupled with a molecular junction [141].

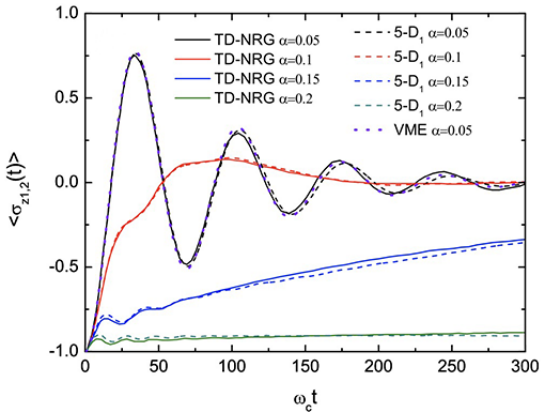


Figure 6: Time evolution of the population difference of two spins coupled to a common bath with $s = 1$ and various coupling constants $\alpha$. Other parameters are $\Delta_1 = \Delta_2 = 0.1\omega_c$, $V = 0.05\omega_c$. The perturbative results are presented only for the moderately weak coupling strengths.

The existence of three phases, the "localized phase," the "critical phase," and the "free phase", has been predicted by a perturbative renormalization group theory, for $s = \bar{s}$, $\alpha = \beta$, and $\varepsilon = \Delta = 0$ [134, 142, 143]. This was later confirmed by numerical means in the strong, the intermediate, and the weak coupling regime [144]. A continuous QPT separating the localized and the critical phase was claimed to exist only for $s^* < s < 1$, and a critical exponent of $s^* = 0.75$ was estimated from DMRG, while for $s > 1$, the impurity behaves as a free spin in the "free phase." [144] Moreover, a critical exponent of $s^* = 1/2$ was recently by a mean-predicted field analysis [35], at variance with the aforementioned DMRG result. Employing the multi-$D_1$ Ansatz, rotational- and parity-symmetry breaking is found to occur along the localized-to-critical phase transition, and a critical spectral exponent of $s^* = 0.49(1)$ is determined, in good agreement with the mean-field predictions [35].

### 6.3 The two-spin spin-boson model

Making use of the multi-$D_1$ Ansatz [61], we have studied a 2-spin SBM with two spins interacting with a common reservoir, the Hamitonian of which is given by

$$\hat{H}_{\rm SBM}^{2-{\rm spin}} = -\sum_{i=1}^{2}\frac{\Delta_i}{2}\sigma_{xi} + V\sigma_{1z}\sigma_{2z} + \sum_l \omega_l b_l^\dagger b_l + \frac{\sigma_{z1}}{2}\sum_l \lambda_l(b_l + b_l^\dagger) + \frac{\sigma_{z2}}{2}\sum_l \tilde{\lambda}_l(b_l + b_l^\dagger), \qquad (55)$$

where $\Delta_i$ is the tunneling amplitude of the $i$th spin, $\sigma_{\mu i}$ ($\mu = x, y, z$) is the $\mu$-component Pauli matrix of the $i$th spin, $b_l$ ($b_l^\dagger$) is the annihilation (creation) operator of the $l$th reservoir mode of frequency $\omega_l$. $\lambda_l$ ($\tilde{\lambda}_l$) is the strength of coupling between spin 1 (2) and the bath. The bath spectral density is given by $J(\omega) = \sum_l \lambda_l^2\delta(\omega - \omega_l) = 2\alpha\omega_c^{1-s}\omega^s\Theta(\omega_c - \omega)$, where $\alpha$ is the dimensionless coupling constant, $s$ is the spectral exponent, $\omega_c$ is the cutoff frequency, and $\Theta(\cdot)$ is the Heaviside step function.

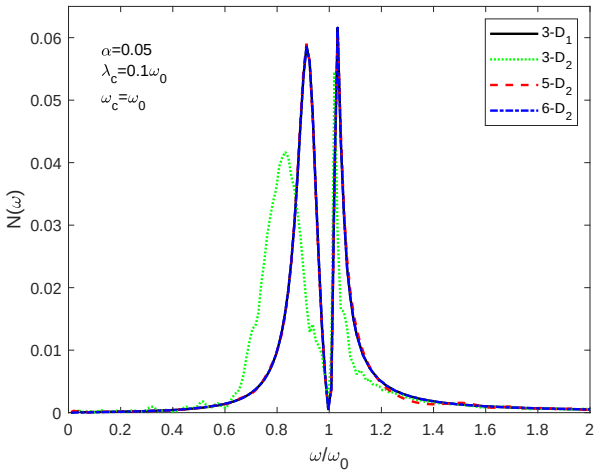


Figure 7: Comparison of emission spectra calculated with the multi-$D_1$ ($M$= 3, or 3-$D_1$) Ansatz and the multi-$D_2$ ($M = 3, 5, 6$) Ansatz, or the , or 3-, 5-, 6-$D_2$ Ansatz.

As shown in Fig. 6, the spin dynamics an Ohmic bath ($s = 1$) have been calculated by the multi-$D_1$ Ansatz, the time-dependent numerical renormalization group (TD-NRG), and the perturbative variational master equation (VME) approach. From weak to strong coupling, the TD-NRG and the multi-$D_1$ results agree with each other. Interestingly, as shown by the two methods, the two spins are found to be localized at strong coupling. But large deviations appear between the two approaches when the two spins are coupled to a sub-Ohmic bath. While it is well known that the application of the NRG to the sub-Ohmic SBM has led to unreliable conclusions regarding quantum critical behavior [145], the relative deviations of the multi-$D_1$ trial states, i.e., Eq. (23), are found to be diminutive in this regime, indicating unambiguously that the multi-$D_1$ results are robust [61].

### 6.4 Vacuum Rabi splitting in a dissipative bath

In this subsection, we consider a model system in which a qubit is coupled simultaneously to a cavity and a radiation bath. The model Hamiltonian is given by

$$\hat{H}_{\rm VRS} = \frac{1}{2}\omega_0\sigma_z + \omega_c b_c^\dagger b_c + \frac{\lambda_c}{2}(b_c + b_c^\dagger)\sigma_x + \sum_k \omega_k b_k^\dagger b_k + \sum_k \frac{\lambda_k}{2}(b_k + b_k^\dagger)\sigma_x, \tag{56}$$

where $\omega_0$ is the qubit energy, $\sigma_i$ ($i = x, y, z$) denotes the Pauli matrices, $b_c$ ($b_c^\dagger$) is the annihilation (creation) operator of the cavity mode of frequency $\omega_c$, $b_k$ ($b_k^\dagger$) is the annihilation (creation) operator of the bath mode of frequency $\omega_k$, $\lambda_c$ and $\lambda_k$ are the cavity- and bath-qubit coupling strengths, respectively. We adopt an Ohmic-type bath spectral density, $J(\omega) = \sum_k \lambda_k^2\delta(\omega_k - \omega) = 2\alpha\omega\exp(-\omega/\omega_{\rm cut})$, where $\alpha$ is the dimensionless coupling constant and $\omega_{\rm cut}$ is the cut-off frequency. The emission spectrum has been calculated using the multi-$D_1$ and multi-$D_2$ Ansätze with a number of multiplicities

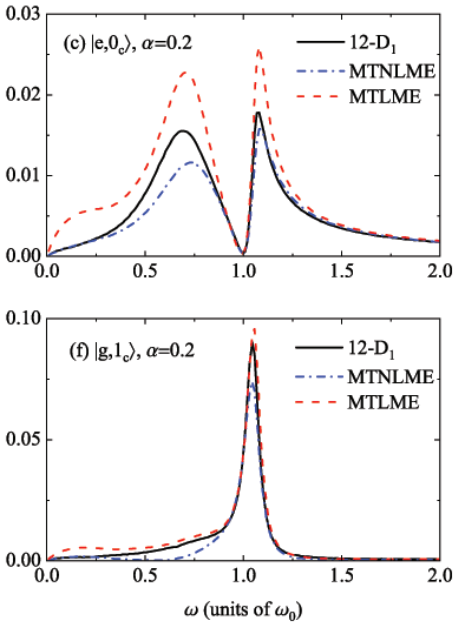


Figure 8: Comparison of emission spectra calculated by the methods of the 12-$D_1$ Ansatz, the modified time-local master equation, and the modified time-nonlocal master equation, for the case of $\alpha = 0.2, \omega_c = \omega_0$, and $\lambda_c = 0.3\omega_0$. Initial states used in the upper and lower panel are $|e, 0_c\rangle$ and $|g, 1_c\rangle$, respectively.

$(M = 3, 5, 6)$, and the results are compared in Fig. 7. As shown in Fig. 7, the vacuum Rabi splitting is clearly visible in the emission spectrum, for the case of $\alpha = 0.05, \omega_c = \omega_0$, and $\lambda_c = \omega_0/10$. One readily notes that the 3-$D_1$ result coincides with the 6-$D_2$ result, which confirms that the multi-$D_1$ state with the multiplicity $M$ is a special case of the multi-$D_2$ states with the multiplicity $2M$ [73].

Due to great succuss in accurately modeling qubit-cavity dynamics of the dissipative Rabi model, multiple Davydov Ansätze are now used to benchmark second-order perturbative methods based on canonical transformations and master equations [146]. Shown in Fig. 8 is a comparison of emission spectra calculated by the multi-$D_1$ Ansatz with $M = 12$, the modified time-local master equation, and the modified time-nonlocal master equation, for the case of $\alpha = 0.2, \omega_c = \omega_0$, and $\lambda_c = 0.3\omega_0$. The initial states used in the upper and lower panel of Fig. 8 are $|e, 0_c\rangle$ and $|g, 1_c\rangle$, respectively, where $|e\rangle$ ($|g\rangle$) is the qubit excited (ground) state and $|n_c\rangle$ $(n = 0, 1)$ is the cavity number state.

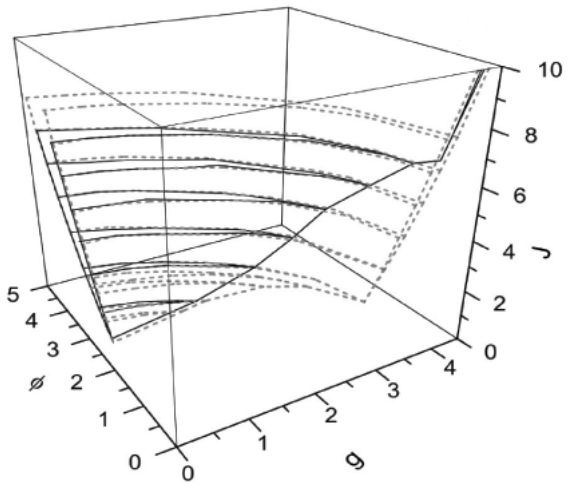


Figure 9: Phase diagram of the near zone-center self-trapping in $g$-$\phi$-$J$ space for the Global-Local Ansatz (solid) and Toyozawa's Ansatz (dashed). In the region under the solid-line ax-shaped curve (where $J$ is small), there is a single solution to the set of self-consistency equations derived from the Global-Local Ansatz, and the transition from small-polaron correlations to large-polaron correlations is smooth. Within the ax-shaped region, the Global-Local Ansatz has two convergent solutions that coexist. For Toyozawa's Ansatz, the region where two solutions coexist is much larger.

# 7 The extended Holstein Hamiltonian

In the original treatment by Holstein, only the site-diagonal exciton-phonon coupling was considered [147, 28, 29], and the site-space Holstein Hamiltonian is written as

$$\begin{aligned} \hat{H}_{\text{Holstein}} &= -J\sum_n a_n^\dagger(a_{n+1}+a_{n-1}) + \omega\sum_n b_n^\dagger b_n + \hat{H}_{\text{ex-ph}}^{\text{diag}}, \\ \hat{H}_{\text{ex-ph}}^{\text{diag}} &= g\omega\sum_n (b_n^\dagger + b_n) a_n^\dagger a_n, \end{aligned} \tag{57}$$

where $J$ is the nearest-neighbor transfer integral, and $\hat{H}_{\text{ex-ph}}^{\text{diag}}$ is the diagonal coupling Hamiltonian with coupling strength $g$. Many of the methods used to study the Fröhlich Hamiltonian have also been applied to the Holstein Hamiltonian. For example, the intermediate coupling theory of Lee, Low, and Pines (LLP) [148], which was developed in 1953 for the Fröhlich Hamiltonian, was subsequently employed by Merrifield [26] to treat the Holstein molecular crystal model, Eq. (57). In place of the LLP transformation, which eliminates the exciton coordinate from Eq. (57), accurate, momentum-conserving variational wave functions, such as Toyozawa's Ansatz and the Global-Local Ansatz, can be utilized to describ the ground state properties of Eq. (57). Additionally, the delocalized $D_1$ Ansatz, $|\Psi_{\text{dD}_1}^K\rangle$ of Eq. (9), has been found to be considerably more accurate than the two aforementioned Ansätze, producing ground state energies of an accuracy rivaling that of the much more computationally demanding DMRG method (cf. Table I of Ref. [34]).

Off-diagonal coupling is the dependence of the transfer integral on nuclear coordinates, which is also known as "nonlocal coupling." Optical and transport properties of molecular systems are strongly

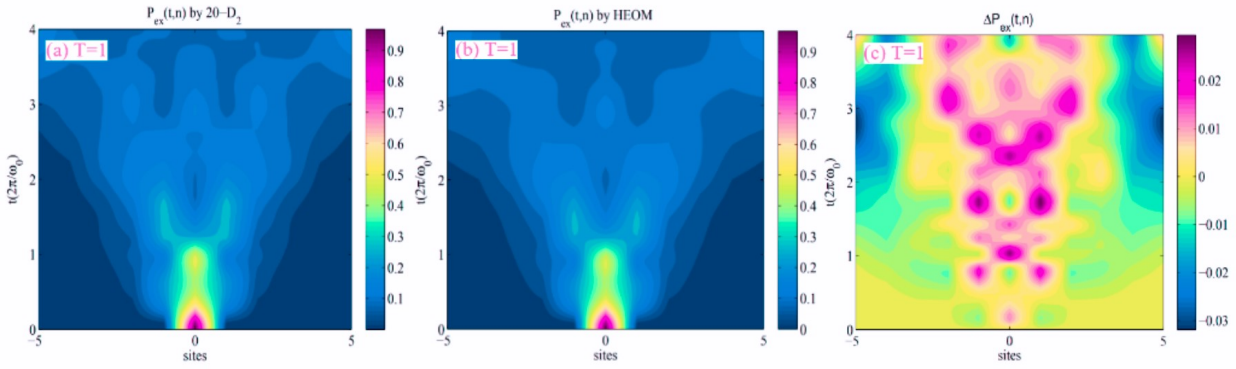


Figure 10: Time dependence of the exciton probability $P_{\rm ex}(t,n)$ for a parameter set of $T=1, J=0.1, W=0, g=0, \phi=0.3$ for a lattice of 10 sites, obtained with (a) the $\mathrm{D}_2^{M=20}$ Ansatz and (b) the HEOM method. The difference in $P_{\rm ex}(t,n)$ between (a) and (b), labelled as $\Delta P_{\rm ex}(t,n)$, is shown in panel (c).

influenced by off-diagonal coupling; in particular, it is believed that off-diagonal coupling plays a dominant role in how transport species are scattered in aromatic hydrocarbon crystals [149, 150, 151, 152, 153], in the $V_k$ center in alkali halides [154, 155], in antiferromagnetic semiconductors [156], and in excimer spectra [157]. But off-diagonal coupling is customarily omitted due to difficulties in achieving reliable solutions [158]. It has been demonstrated that the HDA methodology can treat off-diagonal coupling to any desired precision by increasing the complexity in the Ansatz [60, 37, 159, 118]. Fig. 9 displays the phase diagram of the near zone-center self-trapping in $g$-$\phi$-$J$ space for the Global-Local Ansatz (solid) and Toyozawa's Ansatz (dashed). In the region under the solid-line ax-shaped curve (where $J$ is small), there is a single solution to the set of self-consistency equations derived from the Global-Local Ansatz, and the transition from small- to large-polaron correlations is smooth. Within the ax-shaped region, the Global-Local Ansatz has two convergent solutions that coexist. For Toyozawa's Ansatz, the region where two solutions coexist is much greater. In general, as the variational trial state becomes more sophisticated by adopting more variational parameters, the space of multiple coexisting solutions grows smaller, inferring the absence of formal QPTs in the Holstein systems.

Various types of entanglement in Eq. (57) have been evaluated using Toyozawa's Ansatz [160, 161]. For exmaple, it has been shown that analyzing the quantum entanglement between excitonic and phononic DOFs leads to effective characterization of the small and large polaron regimes [161]. The small (large) polaron regime corresponds to a high (low) level of bipartite exciton-phonon entanglement. Additionally, decreasing the coupling strength through the self-trapping line triggers a sudden drop in the exciton-phonon entanglement. In the presence of off-diagonal coupling, self-trapping

occurs with significant changes in entanglement at both the Brillouin-zone center and edge. [160].

By combining the TFD method with the variation scheme employing the multi-$D_2$ Ansatz, the finite-temperature dynamics of a Holstein polaron can be unveiled with high precision [79]. Using the HEOM result as a banchmark [162], it has been convincingly shown that the finite-temperature variation with the multi-$D_2$ Ansatz is an efficient and reliable apparatus to describe the dynamics of the Holstein polaron at any temperature and in the presence of off-diagonal coupling, as illustrated in Fig. 10 for a lattice of 10 sites. The discrepancy between the multi-$D_2$ Ansatz of multiplicity 20 and the HEOM method is shown to be negligible in Fig. 10 (c). It has been known that an increase in temperature may inhibit polaron mobility for weak to moderate diagonal coupling. By combining the multi-$D_2$ Ansatz with the TFD method, it can be clearly shown that off-diagonal coupling can also lead to phonon-assisted transport that becomes dominant at high temperatures.

# 8 Dynamics of cavity-assisted SF

SF is a spin-allowed process of exciton multiplication in which a singlet exciton splits into two triplet excitations of roughly half the energy of their singlet parent. Much attention has surrounded SF as a potential enabler of photovoltaic devices to bypass the Shockley-Queisser limit in conversion efficiency [163]. There are several factors that can affect the dynamics of SF, such as molecular modes that are coupled to electronic excitations. These modes are shown to play a dominant role in the SF process according to recent theoretical estimates [164, 165] and ultrafast spectroscopic measurements [166, 167, 168]. It was demonstrated that efficient fission in pentacene derivatives [169, 170, 171] and crystalline tetracene [172, 173] has been facilitated by high-frequency phonon modes via vibronic resonances. Using the multi-$D_2$ Ansatz, it has been revealed that additional channels for rapid intramolecular SF [174] can be established by high frequency modes off-diagonally coupled to electronic DOFs. Insufficient attention has been devoted to CIs mediated SF dynamics in molecular systems such as pentacene, tetracene, and rubrene crystals and thin films. Meanwhile, much interest is emerging in hybrid light-matter states in molecular/materials sciences, in which strong light-matter interactions come into existence by coupling cavity photonic modes with various electronic/vibrational DOFs of molecular species. It is logical to merge the best of both worlds by harnessing cavities to improve SF as it has unequivocally been demonstrated in the lab that CI-mediated SF processes in rubrene can be engineered by microcavities [175, 176, 177].

Previously, measured linear/nonlinear spectral signals were interpreted only in terms of model Hamiltonians such as the Holstein-Tavis-Cummings (HTC) model and the Fermi Golden Rule, which do not adequately capture the dynamics of CI-driven SF in microcavities. In addition, the current

understanding of phonon-assisted SF mechanisms is inadequate. To gain dynamic information on population transfer and spectral relaxation, a more realistic model system, e.g., an *ab initio* exciton model, needs to be considered [178, 179, 180, 181]. Multiple Davydov Ansätze come handy in this respect to offer an accurate, efficient description for the exciton-phonon dynamics with many DOFs, producing associated nonlinear response functions and spectroscopic signals with great precision [74, 105, 174, 182].

Let us consider, as an example, two rubrene dimers embedded in an optical cavity and coupled to a cavity photon mode, which can be described by the Hamiltonian $H = \sum_{j=1,2} H_{\rm M}^{(j)} + H_{\rm C} + H_{\rm CM}^{(j)}$. Here $H_{\rm M}^{(j)}$ represents the $j$th pristine dimer, $H_{\rm C}$ refers to the cavity-field Hamiltonian ($H_{\rm C} = \omega_{\rm C} C^\dagger C$ with $C^\dagger$ ($C$) being the photon creation (annihilation) operator with frequency $\omega_{\rm C}$), and $H_{\rm CM}^{(j)}$ specifies the dimer-cavity interaction. In the diabatic representation, each rubrene dimer is represented by a five-electronic-state, two-vibrational-mode system,

$$\begin{aligned} H_{\rm M}^{(j)} &= \sum_{k=g^{(j)},S_1^{(j)},TT^{(j)},S_n^{(j)},TT_n^{(j)}} |k^{(j)}\rangle(\varepsilon_k + h_k^{(j)})\langle k^{(j)}| \\ &+ (|S_1^{(j)}\rangle\langle TT^{(j)}| + |TT^{(j)}\rangle\langle S_1^{(j)}|)\lambda Q_{cu}^{(j)}. \end{aligned} \tag{58}$$

Here $|g^{(j)}\rangle$ is the ground state of $j$th dimer, $|S_1^{(j)}\rangle$ is the singlet electronic state coupled to the triplet-pair state $|TT^{(j)}\rangle$, while $|S_n^{(j)}\rangle$ and $|TT_n^{(j)}\rangle$ are higher-lying singlet and triplet states, respectively. $\lambda$ is the coupling constant specifying the $|S_1\rangle$-$|TT\rangle$ CI responsible for the SF, $\varepsilon_k$ are the electronic energies, and $h_k^{(j)}$ are the phonon Hamiltonians including one interstate coupling mode (subscript c) and one primary tuning mode (subscript t):

$$h_k^{(j)} = h_g^{(j)} + \kappa_k Q_{\rm t}^{(j)},$$

$$h_g = \frac{1}{2}\sum_{\alpha={\rm c,t}} \omega_\alpha([P_\alpha^{(j)}]^2 + [Q_\alpha^{(j)}]^2)$$

Here $\hbar = 1$, $Q_\alpha^{(j)}$ and $P_\alpha^{(j)}$ are, respectively, dimensionless coordinates and momenta of the interstate coupling ($\alpha = {\rm c}$) and tuning ($\alpha = {\rm t}$) modes with frequencies $\omega_\alpha$, and $\kappa_k$ are the intrastate coupling strengths. An effective model of CI-mediated SF has been established in Refs. [183, 182, 184, 185], where the tuning mode $Q_{\rm t}$ is the dimensionless SF reaction coordinate, and $Q_{\rm c}$ is an antisymmetric interstate coupling mode linking the states $|S_1^{(j)}\rangle$ and $|TT^{(j)}\rangle$. Our model here is augmented with the inclusion of the higher-lying $|TT_n^{(j)}\rangle$ and $|S_n^{(j)}\rangle$, which routinely appear in spectroscopic signals simulation of molecular systems [186]. Within the dipole approximation and the rotating wave approximation, the dimer-cavity-photon interaction Hamiltonian reads $H_{\rm CM}^{(j)} = \frac{\Omega}{2}(CX^\dagger + C^\dagger X)$, where $X^\dagger = |S_1^{(j)}\rangle\langle g^{(j)}| + \eta_S |S_n^{(j)}\rangle\langle S_1^{(j)}| + \eta_T |TT_n^{(j)}\rangle\langle TT^{(j)}|$, and $\Omega$ is the vacuum Rabi frequency

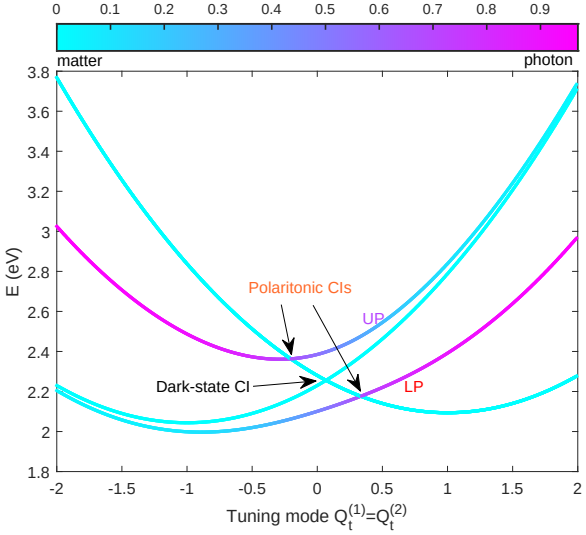


Figure 11: Collective polaritonic PESs at $Q_{\rm c}^{(1)} = Q_{\rm c}^{(2)} = 0$ along the symmetric tuning mode in the singly-excited manifold.

for a molecular emitter. The Rabi splitting of $N$ identical molecules in the cavity is approximately $\Delta_R = \sqrt{(\omega_C - \varepsilon_{S_1})^2 + N\Omega^2}$ in the Franck-Condon regime (see, e.g., Ref. [187]). The state $S_1^{(j)}$ ($TT^{(j)}$) is optically bright (dark), and only the $S_1^{(j)}$ state is coupled to the cavity. $\eta_S$ and $\eta_T$ control the cavity-induced transitions $S_1^{(j)}$-$S_n^{(j)}$ and $TT^{(j)}$-$TT_n^{(j)}$.

The total number of excitations is conserved as the number operator $N_{\rm ex} = C^\dagger C + \sum_{j,k} |k^{(j)}\rangle\langle k^{(j)}|$ commutes with the system Hamiltonian $H$. The two identical dimers have their Hamiltonians parameterized according to Refs. [183, 182, 184, 185]: $\varepsilon_{S_1} = 2.23$ eV, $\varepsilon_{TT} = 2.28$ eV, $\omega_{\rm t} = 0.186$ eV, $\omega_{\rm c} = 0.0154$ eV, $\kappa_{S_1} = 0.372$ eV, $\kappa_{TT} = -0.372$ eV, and $\lambda = 0.0745$ eV. Only tentative energy assignments are available for higher-lying singlet and triplet states [183, 188, 189, 190, 191, 192]. Following Ref. [183] we set $\varepsilon_{S_n} = 4.33$ eV and $\varepsilon_{TT_n} = 4.68$ eV. It is also reasonable to assume that $\kappa_{S_n} = \kappa_{S_1}$ and $\kappa_{TT_n} = \kappa_{TT}$. Identical transition dipole moments are assumed for all allowed transitions, and $\eta_S = \eta_T = 1$ is set. The cavity mode is given a frequency of $\omega_C = 2.256$ eV, matching the pristine CI position (without cavity). It is also almost in electronic resonance with the bright $S_1^{(j)}$ state. We set $\Omega = 0.2$ eV, which leaves the cavity-matter interaction in the strong-coupling regime.

We first consider the singly-excited manifold of $\langle N_{\rm ex}\rangle = 1$, where the state vectors span a 5-dimensional space with the basis set $|1_C, g^{(1)}, g^{(2)}\rangle$, $|0_C, S_1^{(1)}, g^{(2)}\rangle$, $|0_C, TT^{(1)}, g^{(2)}\rangle$, $|0_C, g^{(1)}, S_1^{(2)}\rangle$, and $|0_C, g^{(1)}, TT^{(2)}\rangle$ (the cavity states are labeled as $|i_C\rangle$, where $i = 0, 1, 2$ numbers the cavity photons). Displayed in Fig. 11 are the collective cuts along the symmetric tuning mode $Q_{\rm t}^{(1)} = Q_{\rm t}^{(2)}$ through adiabatic polaritonic PESs. Gradient color lines are used to mark the polaritonic nature

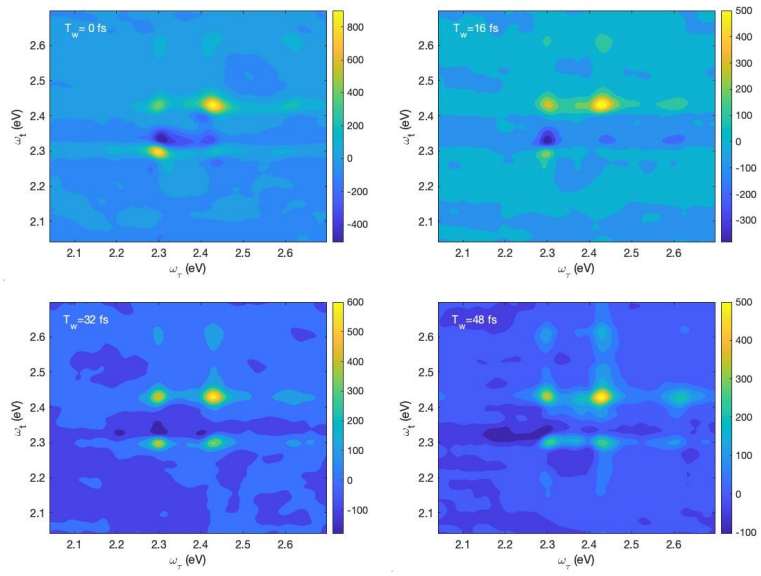


Figure 12: Real part of the 2DES spectrum of the cavity-assisted SF system, computed in the impulsive limit for a few population times, $T_w = 0, 16, 32, 48$ fs (as indicated in the panels). An electronic dephasing time of $\tau_d \sim 125.7$ fs is used.

of these states. There are one dark-state CI and two bright-state polaritonic CIs. Located at $E = 2.256$ eV and $Q_{\rm t}^{(1)} = Q_{\rm t}^{(2)} = 0.07$, the dark-state CI is formed by the states decoupled from the cavity mode, coinciding with the cavity-free CI of the rubrene dimer [183, 182, 184, 185]. The two polaritonic CIs originate in the dimer-cavity coupling. Due to two dimers being identical and their individual electronic states being doubly generate, the collective excitonic states can be expressed as symmetrized/antisymmetrized combinations of these states.

Aside from SF energetics, the Davydov Ansatz methodology can also accurately simulate all other dynamic observables and spectroscopic signals. In CI models with reduced dimensionality, a dephasing time, represented by $\tau_d$, accounts for factors such as temperature, environmental perturbations, and the vibronic density of states. The value of $\tau_d$ is typically between several dozen and a few hundred femtoseconds [193, 38]. Simulated 2D electronic spectra (2DES) $S(\omega_\tau, T_w, \omega_t)$ at a few population times, $T_w = 0, 16, 32, 48$ fs, are presented in Fig. 12, which has two pronounced diagonal peaks (DPs) and two cross peaks (CPs). The diagonal peaks, DP1 ($\omega_\tau = 2.297$ eV, $\omega_t = 2.297$ eV) and DP2 ($\omega_\tau = 2.429$ eV, $\omega_t = 2.429$ eV) reveal the middle polariton (MP) and the upper polariton (UP) bands, respectively, while the cross peaks, CP1 ($\omega_\tau = 2.429$ eV, $\omega_t = 2.297$ eV) and CP2 ($\omega_\tau = 2.297$ eV, $\omega_t = 2.429$ eV) quantify the coupling and polaritonic coherence between the MP and UP states.

# 9 Conclusions and Discussion

In this Perspective, I give an overview of the past decade's developments of the family of Davydov's Ansätze with applications to a few many-body quantum systems of interest in chemical physics. It has been demonstrated that the Davydov Ansätze, in combination with standard time-dependent variation and its finite-temperature extensions, offer an all-around toolbox for numerically efficient, accurate evaluations of dynamic and spectroscopic properties of a large variety of many-body problems. Initially proposed as possible carriers of vibrational energy in proteins, Davydov's solitons after undergoing momentum-space projection were found to provide great approximations to the ground-state wave functions of the generalized Holstein Hamiltonian [29, 34], inferring the absence of QPTs in the Holstein systems [194, 195]. Pioneered by Shore and Sander half a century ago, the multiple Davydov Ansätze were developed as improved versions of their single-Ansatz counterparts, allowing for incrementally more accurate descriptions of the nuclear DOFs of the many-body wave functions. For sufficiently large multiplicities, one achieves a numerically "exact" solution to the many-body Schrödinger equation in the form of the multiple Davydov Ansätze, two versions of which, namely, the multi-$D_1$ and the multi-$D_2$ Ansätze, have been implemented, with great success, to several many-body quantum systems of broad interest, including the SBM variants [36, 61, 60, 196], dissipative Landau-Zener transitions [197], and the generalized Holstein molecular crystal model in 1D [32, 34, 37, 79] and 2D [198].

Nonperturbative, numerically "exact" for large Ansatz multiplicities, the multiple Davydov Ansätze are also capable to handle dynamic properties of large, realistic materials systems and extract multidimensional spectroscopic signals for close comparison with experiment [74, 105]. As a practical application, the variational HDA method has been used to simulate many-body dynamics and nonlinear spectroscopic signatures of cavity-assisted, CI-controlled SF systems, an example of which in rubrene has been discussed in great detail in this Perspective [176, 177]. With algorithmic implementation in graphic processing units, the Davydov trial states have also been applied to efficiently model exciton-phonon dynamics in mesoscale light-harvesting systems containing more than 1600 pigments [199], highlighting the capability of the HDA methodology in accurate simulation of large-system quantum dynamics. In addition, Zheng *et al.* have adopted the multi-$D_2$ Ansatz to explore the composite photon-qubit-phonon dynamics in hybrid circuit quantum electrodynamics (QED) devices [200, 201, 202, 203]. Thanks to explicit treatments of individual bosonic DOFs within the HDA framework, involvement of all photon/phonon modes in the system dynamics can be unveiled clearly, facilitating photonic-state engineering in QED devices in quantum information and computation. Most recently, by constructing *ab initio*-parametrized multispecies Hamiltonians, the HDA approach

has been successfully utilized to investigate exciton dynamics and time- and frequency-resolved fluorescence spectra in nanocavity-integrated monolayers of transition metal dichalcogenides (TMD) [204], establishing dynamical and spectroscopic signatures of the polaronic and polaritonic effects in these extremely promising, atomically thin semiconductors. To my knowledge, among all materials systems whose dynamic and spectroscopic properties have been simulated by a numerically accurate, fully quantum method at finite temperatures, the TMD monolayers are the most complex, challenging multidimensional CI construct. Our HDA study reveals the pivotal role of multidimensional CIs in controlling the many-body dynamics of highly intertwined excitonic, phononic, and photonic modes in complex materials systems.

The HDA approach belongs to a large family of methods which involve Gaussian basis functions in solving the Schrödinger equation in a multidimensional Hilbert space, a body of work that can be traced back to the semiclassical thawed Gaussian approximation [205] and the frozen Gaussian approximation [206, 207]. In the thawed Gaussian approximation, the center of a Gaussian wave packet follows the Newtonian dynamics, but its width is adjusted based on an effective potential derived from truncating the PES around the center of the Gaussian at second order. In the frozen Gaussian approximation, the wave-packet width remains constant, and the PES nonlinearity is accounted for approximately. The MS method of Martínez and coworkers [57, 58, 208] adopts adaptive linear superpositions of Gaussian basis sets that follow classical trajectories, where the set of Gaussian basis functions can expand via a process called "spawning," designed to more accurately capture nonadiabatic dynamics at coupled PESs and/or tunneling effects. The variational multi-configurational Gaussian (vMCG) approach of Burghardt and coworkers [209, 70], analogous to the HDA methodology, solves coupled EOMs for the Gaussian parameters via time-dependent variation. Werther and Grossmann invented an "apoptosis" procedure removing quasi-degenerate Gaussian wave packets [210, 211] during wave-function propagation. The coupled-coherent states (CCS) method developed by Shalashilin and co-workers [69, 212, 213, 214] uses nuclear wave functions in a basis of trajectory-guided Gaussians evolving on an averaged quantum potential. Extension of the CSS method to include multiple coupled PESs leads to the multiconfigurational Ehrenfest (MCE) method [65, 66, 220]. The Hagedorn wave packets [215, 216] and the generalized coherent state method [62, 67, 217] employ products of Gaussians and multi-dimensional polynomials as basis functions. The aforementioned Gaussian methods may differ in the detailed basis-function choices and in the specific methods of solutions for the variational parameters. Nonetheless, the common Gaussian basis functions often allow for smooth migration of the tools developed within the HDA formalism to other Gaussian methods and vice versa. For instance, the HDA approach to the computation of multidimensional

spectroscopic signals [59, 104] was transferred to the MCE framework [218, 219]. While it is hard to exhaust the likely methodological "exchanges," it would be promising to extend the HDA machinery of evaluating multidimensional diabatic/adiabatic wave packets [64] to other Gaussian methods, and to combine the Davydov Ansätze with methods of *ab initio* electronic-structure calculations for on-the-fly dynamics simulations by adopting techniques from, for example, the *ab initio* MS (AIMS) [221], the external-field AIMS [222, 223], the *ab initio* multiple cloning (AIMC) [224], and the direct dynamics variant of vMCG [225].

To conclude, the HDA methodology and its finite-temperature extensions offer practitioners of quantum simulations with an accurate, effective tool for evaluating multiple-species, many-body dynamics together with multidimensional, fully quantum spectroscopic signals, including both transient and steady-state responses, for a wide range of many-body particle-boson systems in chemical physics. It is promising to use the HDA machinery to probe the femtosecond dynamics of cavity QED systems and atomically thin, novel semiconductors in order to to untangle fascinating dynamic intricacies of intertwined excitonic, phononic, and photonic modes in complex materials systems in the presence of quantum light. It is also a challenging task to employ the HDA methodology to study nonlinear and mode-mode coupling effects in quantum transport and multidimensional spectroscopy, to upgrade the multi-coherent-state description to handle systems with fermionic and rotational DOFs, and to develop state-of-the-art deep-learning techniques to help speed up dynamics simulation of increasingly more complex materials systems [226]. The HDA methodology belongs to the class of variational quantum algorithms (VQAs) that have recently emerged as a leading strategy to address the current constraints of limited qubit numbers and noise processes in quantum computing [227]. VQAs are now being proposed for all applications as they appear as the best hope to secure the quantum computational advantage. In light of this development, the coming years will likely see a much greater level of development of the HDA methodology as well as its application to various many-body problems in chemical physics.

## Acknowledgments

I would like to thank Kewei Sun, Maxim Gelin, Frank Grossmann, Yiying Yan, Lu Wang, Nengji Zhou, Lipeng Chen, Fulu Zheng, Raffaele Borrelli, and Yuta Fujihashi for helpful discussion. Support from the Singapore Ministry of Education Academic Research Fund Tier 1 (Grant No. RG190/18) is gratefully acknowledged.

## Conflict of Interest

The author has declared no conflicts of interest for this article.

## Data Availability

The data that support the findings of this study are available from the corresponding author upon reasonable request.

## References


[1] M.J. Škrinjar, D.V. Kapor, S.D. Stojonović, "Classical and quantum approach to Davydov's soliton theory," *Phys Rev A* **38**, 6402-6407 (1988).

[2] Q. Zhang, V. Romero-Rochin, R. Silbey, "Variational approach to the Davydov soliton," *Phys Rev A* **38**, 6408-6415 (1988).

[3] A.S. Davydov, "The theory of contraction of proteins under their excitation," *J Theor Biol.* **38**, 559-569(1973).

[4] A.S. Davydov, "Theory of Molecular Excitons," Plenum Press, New York-London, 1971.

[5] A.S. Davydov, "Deformation of Molecular Crystals at Electronic Excitation," *Phys Stat Sol.* **36**, 211-219 (1969).

[6] A.S. Davydov and N. Kislukha, " Solitary excitons in one-dimensional molecular chains," *Phys. Stat. Sol.* **59**, 465-470 (1973).

[7] A.S. Davydov, "Dvizhenie solitona v odnomernoi molekulyarnoi reshetke s uchetom teplovih kolebanii," *Zh. Eksp. Teor. Fiz.* **78**, 789 (1980).

[8] A.C. Scott, "Davydov's soliton," *Phys. Rep.* **217**, 1-67(1992).

[9] A.C. Scott, "The laser-Raman spectrum of a Davydov soliton," *Phys. Lett. A* **86**, 60-62 (1981).

[10] G. Careri, U. Buontempo, F. Carta, E. Gratton, and A.C. Scott, "Infrared Absorption in Acetanilide by Solitons", *Phys. Rev. Lett.* **51**, 304 (1983).

[11] M. Satarić, Z. Ivić, and R. Žakula, "The temperature dependence of excitonphonon coupling in the context of Davydovs model: the dynamic damping of soliton," in: Davydovs Soliton Revisited, eds. P.L. Christiansen and A.C. Scott, Plenum, New York, 1990.

[12] A.C. Scott, "Dynamics of Davydov solitons," *Phys. Rev. A* **26**, 578 (1982).

[13] W. Förner, "Davydov solition dynamics-temperature effects," *J. Phys. Cond. Matt.* **3**, 4333-4348 (1991).

[14] W. Förner, "Davydov solition dynamics: Initial state, boundary conditions, and numerical procedure," *J. Comp. Chem.* **13**, 275-313 (1992).

[15] W. Förner, "Quantum and temperature effects on Davydov soliton dynamics. III. Interchain coupling," *J. Phys. Cond. Matt.* **5**, 823-840 (1993).

[16] X. Wang, D.W. Brown, and K. Lindenberg, "Quantum Monte Carlo Simulations of the Davydov Model," *Phys. Rev. Lett.* **62**, 1796 (1989).

[17] X. Wang, D.W. Brown, and D.K. Campbell, "Equivalence of the Holstein Polaron to an One-Dimension Classical Gas," *Phys. Lett. A* **181**, 123-128 (1993).

[18] P.S. Limdahl and W.C. Kerr, "Do Davydov Solitons Exist at 300 K?" *Phys. Rev. Lett.* **55**, 1235-1238 (1985).

[19] L. Bernstein L, J.C. Eilbeck, and A.C. Scott, "The quantum theory of local modes in a coupled system of nonlinear oscillators. *Nonlinearity* **3**, 293 (1990).

[20] Y. Zhao Y and D.W. Brown, "Robustness of the single dressing fraction characterization of polaron structure in multi-mode partial dressing theory," *J. Lumin.* **58**, 61-65 (1994).

[21] M. Plodzien, T. Sowinski, and S. Kokkelmans, "Simulating polaron biophysics with Rydberg atoms," *Sci. Rep.* **8**, 9247 (2018).

[22] D.D. Georgiev, J.F. Glazebrook, "On the quantum dynamics of Davydov solitons in protein alpha-helices," *Physica A* **517**, 257-269 (2019).

[23] O.O. Vakhnenko, "Nolinear integrable dynamics of coupled vibrational and intra-site excitations on a regular one-dimensional lattice," Phys. Lett. A **405**, 127431 (2021).

[24] V. Čápek and D. Krausová, "To the relation between energies of molecular soliton and extended states in chains," *Czech. J. Phys. B* **37**, 1201-1202 (1987).

[25] Y. Toyozawa, "Self-Trapping of an Electron by the Acoustical Mode of Lattice Vibration. I.," *Prog. Theor. Phys.* **26**, 29-44 (1961).

[26] R.E. Merrifield, "Theory of the Vibrational Structure of Molecular Exciton States," *J. Chem. Phys.* **40**, 445 (1964).

[27] H.B. Shore and L.M. Sander, "Ground State of the Exciton-Phonon System," *Phys. Rev. B***7**, 4537 (1973).

[28] G. Venzl and S.F. Fischer, "Theory of exciton-phonon coupling in one-dimensional molecular crystals: A variational treatment with delocalized solitary states. *Phys. Rev. B* **32**, 6437 (1985).

[29] Y. Zhao, *Doctoral thesis*, University of California, San Diego, 1994.

[30] Y. Zhao, D.W. Brown, and K. Lindenberg, "A Variational Approach to Nonlocal Exciton-Phonon Coupling," *J. Chem. Phys.* **106**, 2728 (1997).

[31] Y. Zhao, D.W. Brown, and K. Lindenberg, "Variational Energy Band Theory for Polarons: Mapping Polaron Structure with the Merrifield Method," *J. Chem. Phys.* **106**, 5622 (1997).

[32] Y. Zhao, D.W. Brown, and K. Lindenberg, "Variational Energy Band Theory for Polarons: Mapping Polaron Structure with the Toyozawa Method," *J. Chem. Phys.* **107**, 3159 (1997).

[33] Y. Zhao, D.W. Brown, and K. Lindenberg, "Variational Energy Band Theory for Polarons: Mapping Polaron Structure with the Global-Local Method. *J. Chem. Phys.* **107**, 3179 (1997).

[34] J. Sun J, L. Duan L, and Y. Zhao, "Delocalized Davydov $D_1$ Ansatz for the Holstein Polaron," *J. Chem. Phys.* **138**, 174116 (2013).

[35] N. Zhou, L. Chen, Y. Zhao, D. Mozyrsky, V. Chernyak, and Y. Zhao, "Ground state properties of sub-Ohmic spin-boson model with simultaneous diagonal and off-diagonal coupling," *Phys. Rev. B* **90**, 155135 (2014).

[36] L. Wang, L. Chen, N. Zhou, and Y. Zhao, "Variational dynamics of the sub-Ohmic spin-boson model on the basis of multiple Davydov $D_1$ states," *J. Chem. Phys.* **144**, 024101 (2016).

[37] N. Zhou, L. Chen, Z. Huang, Y. Tanimura, and Y. Zhao, "Fast, accurate simulation of polaron dynamics and multidimensional spectroscopy by multiple davydov trial state," *J. Phys. Chem. A* **120**, 1562-1576 (2016).

[38] K.W. Sun, W.W. Xie, L.P. Chen, W. Domcke, M.F. Gelin, "Multi-faceted spectroscopic mapping of ultrafast nonadiabatic dynamics near conical intersections: A computational study," *J. Chem. Phys.* **153**, 174111 (2020).

[39] M. Jakucionis, T. Mancal, and D. Abramavicious, "Modeling irreversible molecular internal conversion using the time-dependent variational approach with $sD_2$ Ansatz," *Phys. Chem. Chem. Phys.* **22**, 8952-8962 (2020).

[40] J. Zeng and Y. Yao, "Variational squeezed Davydov Ansatz for realistic chemical Systems with nonlinear vibronic coupling," *J. Chem. Theory Comput.* **18**, 1255-1263 (2022).

[41] S. Mukamel, "Principles of Nonlinear Optical Spectroscopy," Oxford University Press, New York, 1995.

[42] Y. Tanimura, "Stochastic Liouville, Langevin, Fokker-Planck, and master equation approaches to quantum dissipative systems," *J. Phys. Soc. Jpn.* **75**, 082001 (2006).

[43] Y. Tanimura, "Numerically "exact" approach to open quantum dynamics: The hierarchical equations of motion (HEOM)," *J. Chem. Phys.* **153**, 020901 (2020).

[44] N. Makri and D.E. Makarov, "Tensor propagator for iterative quantum time evolution of reduced density matrices. I. Theory," *J. Chem. Phys.* **102**, 4600-4610 (1995).

[45] N. Makri and D.E. Makarov, "Tensor propagator for iterative quantum time evolution of reduced density matrices. II. Numerical methodology," *J. Chem. Phys.* **102**, 4611-4618 (1995).

[46] Y. Tanimura and A. Ishizaki, " Modeling, Calculating, and Analyzing Multidimensional Vibrational Spectroscopy," *Acc. Chem. Res. 42*, 1270-1279 (2009).

[47] Y. Tanimura, "Reduced hierarchy equations of motion approach with Drude plus Brownian spectral distribution: Probing electron transfer processes by means of two-dimensional correlation spectroscopy," *J. Chem. Phys.* **137**, 22A550 (2012).

[48] T. Ikeda and Y. Tanimura, "Probing photoisomerization processes by means of multidimensional electronic spectroscopy: The multi-state quantum hierarchical Fokker-Planck equation approach," *J. Chem. Phys.* **147**, 014102 (2017).

[49] X.T. Liang, "Simulating signatures of two-dimensional electronic spectra of the Fenna-Matthews-Olson complex: By using a numerical path integral," *J. Chem. Phys.* **141**, 044116 (2014).

[50] J. Hu, M. Luo, F. Jiang, R.X. Xu, and Y.J. Yan, "Padé spectrum decompositions of quantum distribution functions and optimal hierarchical equations of motion construction for quantum open systems," *J. Chem. Phys.* **134**, 244106 (2011).

[51] Z. Tang, X.Q. Ouyang, Z. Gong, H. Wang, and J.L. Wu, "Extended hierarchy equations of motion for the spin-boson model," *J. Chem. Phys.* **143**, 224112 (2015).

[52] H. Rahman and U. Kleinekathöfer, "Chebyshev hierarchical equations of motion for systems with arbitrary spectral densities and temperatures," *J. Chem. Phys.* **150**, 244104 (2019).

[53] M.H. Beck, A. Jäckle, G.A. Worth, and H.D. Meyer, "The Multiconfiguration Time-Dependent Hartree (MCTDH) Method: A Highly Efficient Algorithm for Propagating Wave packets," *Phys. Rep.* **324**, 1-105 (2000).

[54] G.A. Worth, and H.D. Meyer, H. Köppel, L.S. Cederbaum, and I. Burghardt, "Using the MCTDH Wavepacket Propagation Method to Describe Multimode Non-Adiabatic Dynamics," *Int. Rev. Phys. Chem.* **27**, 569-606 (2008).

[55] H.B. Wang and M. Thoss, "Multilayer formulation of the multiconfiguration time-dependent Hartree theory," *J. Chem. Phys.* **119**, 1289 (2003).

[56] U. Manthe, "A multilayer multiconfigurational time-dependent Hartree approach for quantum dynamics on general potential energy surfaces," *J. Chem. Phys.* **128**, 164116 (2008).

[57] M. Ben-Nun, T.J. Martínez, "Nonadiabatic Molecular Dynamics: Validation of the Multiple Spawning Method for a Multidimensional Problem," *J. Chem. Phys.* **108**, 7244-7257 (1998).

[58] M. Ben-Nun, T.J. Martínez, "A multiple spawning approach to tunneling dynamics, *J. Chem. Phys.* **1128**, 6113-6121 (2000).

[59] T. Huynh, K. Sun, M.F. Gelin, and Y. Zhao, "Polaron dynamics in two-dimensional photon-echo spectroscopy of molecular rings," *J. Chem. Phys.* **139**, 104103 (2013).

[60] N. Zhou N, Z. Huang, J. Zhu, V. Chernyak, and Y. Zhao, "Polaron dynamics with a multitude of Davydov $D_2$ trial states," *J. Chem. Phys.* **143**, 014113 (2015).

[61] T. Deng, Y. Yan, L. Chen, and Y. Zhao, "Dynamics of the two-spin spin-boson model with a common bath," *J. Chem. Phys.* **144**, 144102 (2016).

[62] L. Chen L, R. Borrelli, and Y. Zhao, "Dynamics of Coupled Electron-Boson Systems with the Multiple Davydov $D_1$ Ansatz and the Generalized Coherent State," *J. Phys. Chem. A* **121**, 8757-8770 (2017).

[63] L. Chen L, M.F. Gelin, and Y. Zhao, "Dynamics of the spin-boson model: A comparison of the multiple Davydov $D_1$, $D_{1.5}$, $D_2$ Ansätze," *Chem. Phys.* **515**, 108-118 (2018).

[64] L. Chen L, M.F. Gelin, and W. Domcke, "Multimode quantum dynamics with multiple Davydov $D_2$ trial states: Application to a 24-dimensional conical intersection model," *J. Chem. Phys.* **150**, 024101 (2019).

[65] D.V. Shalashilin, "Quantum mechanics with the basis set guided by Ehrenfest trajectories: Theory and application to spin-boson model," *J. Chem. Phys.* **130**,244101 (2009).

[66] D.V. Shalashilin, "Nonadiabatic dynamics with the help of multiconfigurational Ehrenfest method: Improved theory and fully quantum 24D simulation of pyrazine," *J. Chem. Phys.* **132**, 244111 (2010).

[67] R. Borrelli and M.F. Gelin, "The Generalized Coherent State Ansatz: Application to quantum electron-vibrational dynamics," *Chem. Phys.* **481**, 91-98 (2016).

[68] I. Burghardt, K. Giri, and G.A. Worth, "Multimode quantum dynamics using Gaussian wavepackets: The Gaussian-based multiconfiguration time-dependent Hartree (G-MCTDH) method applied to the absorption spectrum of pyrazine," *J. Chem. Phys.* **129**, 174104 (2008).

[69] D.V. Shalashilin and M.S. Child, "The Phase Space CCS Approach to Quantum and Semiclassical Molecular Dynamics for High-dimensional System," *Chem. Phys.* **304**, 103-120 (2004).

[70] G.W. Richings, I. Polyak, K.E. Spinlove, G.A. Worth, I. Burghardt, and B. Lasorne, "Quantum dynamics simulations using Gaussian wave packets; the vMCG method," *Int. Rev. Phys. Chem.* **34**, 269-308 (2015).

[71] H.B. Wang and M. Thoss, "Quantum-mechanical evaluation of the Boltzmann operator in correlation functions for large molecular systems: A multilayer multiconfiguration time-dependent Hartree approach," *J. Chem. Phys.* **124**, 034114 (2006).

[72] L. Wang, Y. Fujihashi, L. Chen, and Y. Zhao, "Finite-temperature time-dependent variation with multiple Davydov states," *J. Chem. Phys.* **146**, 124127 (2017).

[73] M. Werther M, F. Grossmann F, Z. Huang, and Y. Zhao, "Davydov-Ansatz for Landau-Zener-Stueckelberg-Majorana transitions in an environment: Tuning the survival probability via number state excitation," *J. Chem. Phys.* **150**, 234109 (2019).

[74] W. Hu, K. Sun, Q. Xu, L. Chen, and Y. Zhao, "Ultrafast dynamics in rubrene and its spectroscopic manifestation," *J. Chem. Phys.* **153**, 174105 (2020).

[75] M. Suzuki, "Thermo Field Dynamics in Equilibrium and Non-Equilibrium Interacting Quantum Systems," *J. Phys. Soc. Jpn.* **54**, 4483-4485 (1985).

[76] Y. Takahashi and H. Umezawa, "Thermo Field Dynamics," *Int. J. Mod. Phys. B* **10**, 1755-1805 (1996).

[77] R. Borrelli and M.F. Gelin, "Quantum electron-vibrational dynamics at finite temperature: Thermo field dynamics approach," *J. Chem. Phys.* **145**, 224101 (2016).

[78] R. Borrelli and M.F. Gelin, "Simulation of Quantum Dynamics of Excitonic Systems at Finite Temperature: an efficient method based on Thermo Field Dynamics," *Sci. Rep.* **7**, 9127 (2017).

[79] L. Chen and Y. Zhao, "Finite temperature dynamics of a Holstein polaron: The thermo-field dynamics approach," *J. Chem. Phys.* **147**, 214102 (2017).

[80] C.S. Reddy and M.D. Prasad, "Finite temperature vibronic spectra of harmonic surfaces: a time-dependent coupled cluster approach," *Mol. Phys.* **113**, 3023-3030 (2015).

[81] T. Begušić T and J. Vaníček, "On-the-fly ab initio semiclassical evaluation of vibronic spectra at finite temperature," *J. Chem. Phys.* **153**, 024105 (2020).

[82] G. Harsha, T.M. Henderson, and G.E. Scuseria, "Thermofield theory for finite-temperature quantum chemistry," *J. Chem. Phys.* **150**, 154109 (2019).

[83] G. Harsha,, T.M. Henderson, and G.E. Scuseria, "Thermofield Theory for finite-temperature coupled cluster," *J. Chem. Theory. Comput.* **15**, 6127-6136 (2019).

[84] E.W. Fischer, M. Werther, F. Bouakline, F. Grossmann, and P. Saalfrank, "Non-Markovian vibrational relaxation dynamics at surfaces," *J. Chem. Phys.* **156**, 214702 (2022).

[85] B. Luo, J. Ye, C. Guan, and Y. Zhao, "Validity of time-dependent trial states for the Holstein polaron," *Phys. Chem. Chem. Phys.* **12**, 15073-15084 (2010).

[86] J. Sun, B. Luo, and Y. Zhao, "Dynamics of a one-dimensional Holstein polaron with the Davydov Ansatze," *Phys. Rev. B* **82**, 014305 (2010).

[87] Z. Huang, L. Wang, C. Wu, L. Chen, F. Grossmann, and Y. Zhao, "Polaron dynamics with off-diagonal coupling: beyond the Ehrenfest approximation," *Phys. Chem. Chem. Phys.* **19**, 1655-1668 (2017).

[88] Z. Huang, L. Chen, N. Zhou, and Y. Zhao, "Transient dynamics of a one-dimensional Holstein polaron under the influence of an external electric field," *Ann. Phys.* **529**, 1600367 (2017).

[89] L. Chen, M.F. Gelin, W. Domcke, and Y. Zhao, "Theory of femtosecond coherent double-pump single-molecule spectroscopy: application to light harvesting complexes," *J. Chem. Phys.* **142**, 164106 (2015).

[90] V.E. Zakharov and A.B. Shabat,"Exact theory of two-dimensional self-focusing and one-dimensional self-modulation of waves in nonlinear media," *Zh. Eksp. Theor. Fiz. 61*, 118-134 (1971).

[91] F. Manfouo, T.V. Diffo, M.F.C. Fobasso, E. Baloïtcha, M.N. Hounkonnou, and A.J. Fotue, "Properties of acoustic polaron in free-standing slab," Physica B **643**, 414172 (2022).

[92] T.D. Lee, "Particle Physics and Introduction to Field Theory, Contemporary Concepts in Physics," Vol. 1,Harwood Academic Publishers, New York, 1988.

[93] R.J. Glauber, "Coherent and Incoherent States of the Radiation Field," *Phys. Rev.* **131**, 2766 (1963).

[94] Z. Ivić and D.W. Brown, "Soliton excitations of a small-polaron band," *Phys. Rev. Lett.* **63**, 426 (1989); D.W. Brown and Z. Ivić, "Unification of polaron and soliton theories of exciton transport," *Phys. Rev. B***40**, 9876 (1989).

[95] D. Feinberg, S. Ciuchi, and F. de Pasquale, "Squeezing phenomena in interacting electron-phonon systems," *Int. J. Mod. Phys. B* **4**, 1317-1367 (1990).

[96] M. Werther and F. Grossmann,"The Davydov D1.5 Ansatz for the quantum Rabi mode," *Phys. Scr.* **93**, 074001 (2018).

[97] Y. Yan, L. Chen, J. Luo, and Y. Zhao, "Variational approach to time-dependent fluorescence of a driven qubit," *Phys. Rev. A* **102**, 023714 (2020).

[98] M. Werther and F. Grossmann, "Stabilization of adiabatic population transfer by strong coupling to a phonon bath," *Phys. Rev. A* **102**, 063710 (2020).

[99] T.M. Clarke and J.R. Durrant, "Charge photogeneration in organic solar cells," *Chem. Rev. 110*, 6736-6767 (2010).

[100] L.P. Chen, P. Shenai, F.L. Zheng, A. Somoza, and Y. Zhao," Optimal energy transfer in light-harvesting systems," *Molecules 20*, 15224-15272 (2015).

[101] M.F. Gelin, D. Egorova, and W. Domcke, "Efficient Calculation of Time- and Frequency-Resolved Four-Wave-Mixing Signals," *Acc. Chem. Res.* **42**, 1290-1298 (2009).

[102] V. Chorosajev, T. Marciulionis, D. Abramavicius, "Temporal dynamics of excitonic states with nonlinear electron-vibrational coupling," *J. Chem. Phys.* **147**, 074114 (2017).

[103] M. Cho, "Two-dimensional Optical Spectroscopy," CRC Press, New York, 2009.

[104] K.W. Sun, M.F. Gelin, V. Chernyak V, and Y. Zhao, "Davydov Ansatz as an efficient tool for the simulation of nonlinear optical response of molecular aggregates," *J. Chem. Phys.* **142**, 212448 (2015).

[105] K.W. Sun and Y. Yao, "Beating maps of singlet fission: Simulation of coherent two-dimensional electronic spectroscopy by Davydov Ansatz in organic molecule," *J. Chem. Phys.* **147**, 224905 (2017).

[106] E.C.G. Sudarshan, "Equivalence of Semiclassical and Quantum Mechanical Descriptions of Statistical Light Beams," *Phys. Rev. Lett.* **10**, 277 (1963).

[107] M. Hillery, R.F. O'connell, M.O. Scully, and E.P. Wigner, "Distribution functions in physics: Fundamentals," *Phys. Rep.* **106**, 121-167 (1984).

[108] H. Umezawa, H. Matsumoto, and M. Tachiki, "Thermo field dynamics and condensed states," North-Holland, 1982.

[109] I. Ojima, "Gauge fields at finite temperatures-Thermo field dynamics and the KMS condition and their extension to gauge theories," *Ann. Phys.* **137**, 1-32 (1981).

[110] M. Suzuki, "Density matrix formalism, double-space and thermo field dynamics in nonequilibrium dissipative systems," *Int. J. Mod. Phys. B* **5**, 1821-1842 (1991).

[111] I.V. Oseledets, "Tensor-Train Decomposition," *SIAM J. Sci. Comput.* **33**, 2295-2317 (2011).

[112] J. Haegeman, C. Lubich, I. Oseledets, B. Vandereycken, and F. Verstraete, "Unifying time evolution and optimization with matrix product states," *Phys. Rev. B***94**, 165116 (2016)

[113] R. Borrelli and M.F. Gelin MF, "Finite temperature quantum dynamics of complex systems: Integrating thermo-field theories and tensor-train methods," *WIREs Comput Mol Sci.* e1539 (2021).

[114] H. Koppel, W. Domcke, and L.S. Cederbaum, "Multimode Molecular Dynamics Beyond the Born-Oppenheimer Approximation," *Adv. Chem. Phys.* **57**, 59-246 (1984).

[115] W. Domcke and G. Stock, "Theory of Ultrafast Nonadiabatic Excited-State Processes and their Spectroscopic Detection in Real Time," *Adv. Chem. Phys.* **100**, 1-169 (1997).

[116] S. Mukamel and D. Abramavicius, "Many-Body Approaches for Simulating Coherent Nonlinear Spectroscopies of Electronic and Vibrational Excitons," *Chem. Rev.* **104**, 2073-2098 (2004).

[117] D. Abramavicius, B. Palmieri, D.V. Voronine, F. Šanda, and S. Mukamel, "Coherent Multidimensional Optical Spectroscopy of Excitons in Molecular Aggreagtes; Quasiparticle vs Supermolecule Perspective," *Chem. Rev.* **109** 2350-2408 (2009).

[118] D. Chen, J. Ye, H. Zhang, and Y. Zhao, "On the Munn–Silbey approach to polaron transport with off-diagonal coupling and temperature- dependent canonical transformations," *J. Phys. Chem. B* **115**, 5312-5321 (2011).

[119] H. Oberhofer, K. Reuter, J. Blumberger, "Charge Transport in Molecular Materials: An Assessment of Computational Methods," *Chem. Rev.* **117**, 10319-10357 (2017).

[120] M.F. Gelin and R. Borrelli, "Thermal Schröinger Equation: Efficient Tool for Simulati.on of Many-Body Quantum Dynamics at Finite Temperature," *Ann Phys.* **529**, 1700200 (2017).

[121] A.J. Leggett, S. Chakravarty, A.T. Dorsey, M.P.A. Fisher, A. Garg, and W. Zwerger, "Dynamics of the dissipative two-state system," *Rev. Mod. Phys.* **59**, 1-85 (1987).

[122] Z. Lü and H. Zheng, "Quantum dynamics of the dissipative two-state system coupled with a sub-Ohmic bath," *Phys. Rev. B* **75**, 054302 (2007).

[123] Q. Wang Q, A.Y. Hu, and H. Zheng, "Analytical approach to dynamical behavior and phase diagrams in dissipative two-state systems," *Phys. Rev. B* **80**, 214301 (2009).

[124] H.B. Wang and M. Thoss, "From coherent motion to localization: dynamics of the spin-boson model at zero temperature," *New J. Phys.* **10**, 115005 (2008).

[125] H.B. Wang and M. Thoss, "From coherent motion to localization: II. Dynamics of the spin-boson model with sub-Ohmic spectral density at zero temperature. *Chem. Phys.* **370**, 78-86 (2010).

[126] P. Nalbach and M. Thorwart, "Crossover from coherent to incoherent quantum dynamics due to sub-Ohmic dephasing," *Phys. Rev. B* **87**, 014116 (2013).

[127] F. Otterpohl, P. Nalbach, and M. Thorwart, "Hidden phase of the spin-boson model," *Phys. Rev. Lett.* **129**, 120406 (2022).

[128] L. Chen, Y. Yan, M.F. Gelin, and Z. Lü, "Dynamics of the spin-boson model: the effect of bath initial conditions," https://doi.org/10.48550/arXiv.2212.05723.

[129] Z. Lü, L. Duan, X. Li, P.M. Shenai, and Y. Zhao, "Sub-Ohmic spin-boson model with off-diagonal coupling: Ground state properties," *J. Chem. Phys.* **139**, 164103 (2013).

[130] R. Bulla, N. Tong, M. Vojta, "Numerical Renormalization Group for Bosonic Systems and Application to the Sub-Ohmic Spin-Boson Model," *Phys. Rev. Lett.* **91**,170601 (2003); M. Vojta, N. Tong, R. Bulla, "Quantum Phase Transitions in the Sub-Ohmic Spin-Boson Model: Failure of the Quantum-Classical Mapping," *Phys. Rev. Lett.* **94**, 070604 (2005); F.B. Anders, R. Bulla, M. Vojta, "Equilibrium and Nonequilibrium Dynamics of the Sub-Ohmic Spin-Boson Model," *Phys. Rev. Lett.* **98**, 210402 (2007).

[131] Y. Zhao, Y. Yao, V. Chernyak, and Y. Zhao, "Spin-boson model with diagonal and off-diagonal coupling to two independent baths: Ground-state phase transition in the deep sub-Ohmic regime," *J. Chem. Phys.* **140**, 161105 (2014).

[132] N. Zhou, L. Chen, D. Xu, V. Chernyak, and Y. Zhao, "Symmetry and the critical phase of the two-bath spin-boson model: Ground-state properties," *Phys. Rev. B* **91**, 195129 (2015).

[133] V.N. Kotov, J. Oitmaa, and O. Sushkov, "Local magnetic impurities in the two-dimensional quantum Heisenberg antiferromagnet," *Phys. Rev. B* **58**, 8500 (1998).

[134] M. Vojta, C. Buragohai, and S. Sachdev, "Quantum impurity dynamics in two-dimensional antiferromagnets and superconductors," *Phys. Rev. B* **61**, 15152 (2000).

[135] A.H.C. Neto, E. Novais, L. Borda, G. Zaránd, and I. Affleck, "Quantum Magnetic Impurities in Magnetically Ordered Systems," *Phys. Rev. Lett.* **91**, 096401 (2003).

[136] D.V. Khveshchenko, "Quantum impurity models of noisy qubits," *Phys. Rev. B* **69**, 153311 (2004).

[137] J. You and F. Nori, "Superconducting Circuits and Quantum Information," *Physics Today* **58**, 42 (2005).

[138] P.C. Cárdenas, M. Paternostro, and F.L. Semião, "Non-Markovian qubit dynamics in a circuit-QED setup," *Phys. Rev. A* **91**, 022122 (2015).

[139] J. Raftery, D. Sadri, S. Schmidt, H.E. Türeci, and A.A. Houck, "Observation of a Dissipation-Induced Classical to Quantum Transition," *Phys. Rev. A* **4**, 031043 (2014).

[140] J. Liao and L. Kuang, "Generation of entangled coherent states of two cavity fields via coupling to a SQUID-based charge qubit," *J. Phys. B: At. Mol. Opt. Phys.* **40**, 1845 (2007).

[141] T. Ruokola and T. Ojanen, "Thermal conductance in a spin-boson model: Cotunneling and low-temperature properties," *Phys. Rev. B* **83**, 045417 (2011).

[142] A.M. Sengupta, "Spin in a fluctuating field: The Bose(+Fermi) Kondo models," *Phys. Rev. B* **61**, 4041 (2000).

[143] L. Zhu and Q. Si, "Critical local-moment fluctuations in the Bose-Fermi Kondo model," *Phys. Rev. B* **66**, 024426 (2002); G. Zarand and E. Demler, "Quantum phase transitions in the Bose-Fermi Kondo model," *Phys. Rev. B* **66**, 024427 (2002).

[144] C. Guo, A. Weichselbaum, J.V. Delft, and M. Vojta, "Critical and Strong-Coupling Phases in One- and Two-Bath Spin-Boson Models," *Phys. Rev. Lett.* **108**, 160401 (2012).

[145] M. Vojta, "Numerical renormalization group for the sub-Ohmic spin-boson model: A conspiracy of errors," *Phys. Rev. B* **85**, 115113 (2012).

[146] C. Zhang, M. Yu, Y. Yan, L. Chen, Z. Lv, and Y. Zhao, 'Emission spectral non-Markovianity in qubit-cavity systems in the ultrastrong coupling regime," *J. Chem. Phys.* **157**, 214116 (2022).

[147] T. Holstein, "Studies of polaron motion: Part I. The molecular-crystal model," *Ann. Phys.* **8**, 325-342 (1959).

[148] T.D. Lee TD, F.E. Low, and D. Pines,"The Motion of Slow Electrons in a Polar Crystal," *Phys. Rev.* **90**, 297 (1953).

[149] P. Gosar and I. Vilfan, "Phonon-assisted current in organic molecular crystals," *Mol. Phys.* **18**, 49-61 (1970).

[150] H. Sumi, "Origin of temperature-independent electron mobilities in organic molecular crystals. *Sol. Stat. Comm.* **28**, 309-312 (1978); H. Sumi, "Theory of electrical conduction in organic molecular crystals: Temperature-independent mobilities," *J. Chem. Phys.* **70**, 3775 (9179).

[151] A. Madhukar and W. Post, "Exact Solution for the Diffusion of a Particle in a Medium with Site Diagonal and Off-Diagonal Dynamic Disorder," *Phys. Rev. Lett.* **91**, 1424 (1977).

[152] G.G. Roberts, N. Apsley, and R.W. Munn, "Temperature dependent electronic conduction in semiconductors," *Phys. Rep.* **60**, 59-150 (1980).

[153] R.W. Munn and R. Silbey, "Theory of electronic transport in molecular crystals. II. Zeroth order states incorporating nonlocal linear electronCphonon coupling," *J. Chem. Phys.* **83**, 1843 (1985); R.W. Munn and R. Silbey, "Theory of electronic transport in molecular crystals. III. Diffusion coefficient incorporating nonlocal linear electronCphonon coupling," *J. Chem. Phys.* **83**, 1854 (1985).

[154] M. Umehara, "On a Self-Trapped Acoustic Polaron with the Site Diagonal and Site Off-Diagonal Electron-Phonon Interaction," *J. Phys. Soc. Jpn.* **47**, 852-860 (1979).

[155] T.P. Das, A.N. Jette, and R.S. Knox, "Theory of the Optical and Magnetic Properties of the Self-Trapped Hole in Lithium Fluoride," *Phys. Rev.* **134**, A1079 (1964).

[156] M. Umehara, "Importance of the site-off-diagonal electron-phonon interaction on the self-trapped small magnetic polaron," *Phys. Rev. B* **27**, 5669 (1983).

[157] H. Sumi, "Two kinds of excimers in -perylene and pyrene crystals: Origin of Y and V emissions," *Chem. Phys.* **130**, 433-449 (1989).

[158] G.D. Mahan "Many-Particle Physics," Plenum Press, New York, 1981.

[159] Y. Zhao, D.W. Brown, and K. Lindenberg, "On the Munn-Silbey Approach to Nonlocal Exciton-phonon Coupling," *J. Chem. Phys.* **100**, 2335 (1994).

[160] J. Sun, Y. Zhao, and W. Liang, "Self-trapping of polarons with off-diagonal coupling ," *Phys. Rev. B* **79**, 155112 (2009).

[161] Y. Zhao, P. Zanardi, and G. Chen, "Quantum Entanglement and the Self-Trapping Transition in Polaronic Systems," *Phys. Rev. B* **70**, 195113 (2004).

[162] L. Chen, Y. Zhao, and Y. Tanimura, "Dynamics of a One-Dimensional Holstein Polaron with the Hierachical Equations of Motion Approach," *J. Phys. Chem. Lett.* **6**, 3110-3115 (2015).

[163] M.B. Smith and J. Michl, "Singlet Fission," *Chem. Rev.* **110**, 6891-6936 (2010).

[164] T.C. Berkelbach, M.S. Hybertsen, and D.R. Reichman, "Microscopic theory of singlet exciton fission. I. General formulation," *J. Chem. Phys.* **138**, 114102 (2013).

[165] T.C. Berkelbach, M.S. Hybertsen, and D.R. Reichman, "Microscopic theory of singlet exciton fission. II. Application to pentacene dimers and the role of superexchange," *J. Chem. Phys.* **138**, 114103 (2013).

[166] A. Musser, M. Liebel, C. Schnedermann, T. Wende, T. Kehoe, A. Rao, and P. Kukura, "Evidence for conical intersection dynamics mediating ultrafast singlet exciton fission," *Nat. Phys.* **11**,352-357 (2015).

[167] A. Bakulin, S. Morgan, T. Kehoe, M. Wilson, A. Chin, D. Zigmantas, D. Egorova, and A. Rao, "Real-time observation of multiexcitonic states in ultrafast singlet fission using coherent 2D electronic spectroscopy," *Nat. Chem.* **8**, 16-23 (2016).

[168] N. Monahan, D. Sun, H. Tamura, K. Williams, B. Xu, Y. Zhong, B. Kumar, C. Nuckolls, A. Harutyunyan, G. Chen, H. Dai, D. Beljonne, Y. Rao, and X. Zhu, "Dynamics of the triplet-pair state reveals the likely coexistence of coherent and incoherent singlet fission in crystalline hexacene," *Nat. Chem.* **9**, 341-346 (2017).

[169] Y. Fujihashi, L. Chen, A. Ishizaki, J. Wang, and Y. Zhao, "Effect of high-frequency modes on singlet fission dynamics," *J. Chem. Phys.* **146**, 044101 (2017).

[170] R. Tempelaar and D.R. Reichman, "Vibronic exciton theory of singlet fission. I. Linear absorption and the anatomy of the correlated triplet pair state," *J. Chem. Phys.* **146**, 174703 (2017).

[171] R. Tempelaar and D.R. Reichman, 'Vibronic exciton theory of singlet fission. II. Two-dimensional spectroscopic detection of the correlated triplet pair state," *J. Chem. Phys.* **146**, 174704 (2017).

[172] A.F. Morrison and J.M. Herbert, "Evidence for Singlet Fission Driven by Vibronic Coherence in Crystalline Tetracene," *J. Phys. Chem. Lett.* **8**, 1442-1448 (2017).

[173] J. Elenewski, U. Cubeta, E. Ko, and H. Chen, "Functional Mode Singlet Fission Theory," *J. Phys. Chem. C* **121**, 4130-4138 (2017).

[174] Z. Huang, Y. Fujihashi, and Y. Zhao, "Effect of off-diagonal exciton-phonon coupling on intramolecular singlet fission," *J. Phys. Chem. Lett.* **8**, 3306-3312 (2017).

[175] S. Takahashi, K. Watanabe, Y. Matsumoto, "Singlet fission of amorphous rubrene modulated by polariton formation," *J. Chem. Phys.* **151**, 074703 (2019).

[176] K. Sun, M.F. Gelin, and Y. Zhao, "Engineering Cavity Singlet Fission in Rubrene," *J. Phys. Chem. Lett.* **13**, 4090-4097 (2022).

[177] K. Sun, M.F. Gelin, and Y. Zhao, "Accurate Simulation of Spectroscopic Signatures of Cavity-Assisted, Conical-Intersection-Controlled Singlet Fission Processes," *J. Phys. Chem. Lett.* **13**, 4280-4288 (2022).

[178] T. Zeng, R. Hoffmann, and N. Ananth, "The Low-Lying Electronic States of Pentacene and Their Roles in Singlet Fission," *J. Am. Chem. Soc.* **136**, 5755-5764 (2014).

[179] P. Petelenz, M. Snamina, and G. Mazur, "Charge-Transfer States in Pentacene: Dimer versus Crystal," *J. Phys. Chem. C* **119**, 4338-14342 (2015).

[180] P. Petelenz and M. Snamina, "Locally Broken Crystal Symmetry Facilitates Singlet Exciton Fission," *J. Phys. Chem. Lett.* **7**, 1913-1916 (2016).

[181] J. Zirzlmeier, D. Lehnherr, P. Coto, E. Chernick, R. Casillas, B. Basel, M. Thoss, R. Tykwinski, and D. Guldi, "Singlet fission in pentacene dimers," *Proc. Natl. Acad. Sci. USA* **112**, 5325-5330 (2015).

[182] K.W. Sun, Z. Huang, M.F. Gelin, L. Chen, and Y. Zhao, "Monitoring of singlet fission via two-dimensional photon-echo and transient-absorption spectroscopy: Simulations by multiple Davydov trial states," *J. Chem. Phys.* **151**, 114102 (2019).

[183] K. Miyata, Y. Kurashige, K. Watanabe, T. Sugimoto, S. Takahashi, S. Tanaka, J. Takeya, T. Yanai, Y. Matsumoto, "Coherent singlet fission activated by symmetry breaking," *Nat. Chem.* **9**, 983-989 (2017).

[184] W. Wang, K.W. Sun, Q. Xu, L. Chen, and Y. Zhao, "Ultrafast dynamics in rubrene and its spectroscopic manifestation," *J. Chem. Phys.* **153**, 174105 (2020).

[185] K.W. Sun, Q. Xu, L. Chen, M.F. Gelin, and Y. Zhao, "Temperature effects on singlet fission dynamics mediated by a conical intersection," *J. Chem. Phys.* **153**, 194106 (2020).

[186] M.F. Gelin, X. Huang, W. Xie, L. Chen, N. Doslić, and W. Domcke, "Ab Initio Surface-Hopping Simulation of Femtosecond Transient-Absorption Pump-Probe Signals of Nonadiabatic Excited-State Dynamics Using the Doorway–Window Representation," *J. Chem. Theory Comput.* **17**, 2394-2408 (2017).

[187] K.W. Sun, C. Dou, M.F. Gelin, and Y. Zhao, "Dynamics of disordered Tavis–Cummings and Holstein–Tavis–Cummings models," *J. Chem. Phys.* **156**, 024102 (2022).

[188] D.M. Finton, E.A. Wolf, V.S. Zoutenbier, K.A. Ward, and I. Biaggio, "Routes to singlet exciton fission in rubrene crystals and amorphous films," *AIP Advances* **9**, 095027 (2019).

[189] L. Ma, K. Zhang, C. Kloc, H. Sun, M. Michel-Beyerle, G. Gurzadyan, "Singlet fission in rubrene single crystal: direct observation by femtosecond pump–probe spectroscopy," *Phys. Chem. Chem. Phys.* **14**, 8307-8312 (2012).

[190] T. Wu, W. Ni, G. Gurzadyan, and L. Sun, "Singlet fission from upper excited singlet states and polaron formation in rubrene film," *RSC Adv.* **11**, 4639 (2021).

[191] K.A. McGarry, W. Xie, C. Sutton, C. Risko, Y. Wu, V. Young Jr., J.L. Bredas, C. Frisbie, C. Douglas, "Rubrene-Based Single-Crystal Organic Semiconductors: Synthesis, Electronic Structure, and Charge-Transport Properties," *Chem. Mater.* **25**, 2254-2263 (2013).

[192] C. Sutton, N. Tummala, D. Beljonne, and J.L. Bredas, "Singlet Fission in Rubrene Derivatives: Impact of Molecular Packing," *Chem. Mater.* **29**, 2777-2787 (2017).

[193] W. Domcke, D. Yarkony, H. Koppel (Eds.), "Conical Intersections: Theory, Computation and Experiment," World Scientific, Singapore, 2011.

[194] B. Gerlach and H. Löwen, "Proof of the nonexistence of (formal) phase transitions in polaron systems. I.," *Phys. Rev. B* **35**, 4291 (1987)

[195] H. Löwen, "Absence of phase transitions in Holstein systems," *Phys. Rev. B* **37**, 8661 (1988).

[196] X. Qian, C. Zeng, and N. Zhou, "Quantum criticality of the Ohmic spin-boson model in a high dense spectrum: Symmetries, quantum fluctuations and correlations," *Physica A* **580**, 126157 (2021).

[197] Z. Huang and Y. Zhao, "Dynamics of dissipative Landau-Zener transition," *Phys. Rev. A* **97**, 013803 (2018).

[198] Y. Zhao, G. Chen G, and L. Yu, "Lattice and Spin Polarons in Two Dimensions," *J. Chem. Phys.* **113**, 6502-6508 (2000).

[199] F. Zheng, L. Chen, J. Gao, and Y. Zhao, "Fully Quantum Modeling of Exciton Diffusion in Mesoscale Light Harvesting Systems," *Materials* **14**, 3291 (2021).

[200] F. Zheng, Y. Shen, K. Sun, and Y. Zhao, "Photon-assisted LandauZener transitions in a periodically driven Rabi dimer coupled to a dissipative mode," *J. Chem. Phys.* **154**, 044102 (2021).

[201] L. Wang, F. Zheng, J. Wang, F. Großmann, and Y. Zhao, "Schrödinger-Cat States in LandauZenerStückelbergMajorana Interferometry: A Multiple Davydov Ansatz Approach," *J. Phys. Chem. B* **125**, 3184-3196 (2021).

[202] Z. Huang, F. Zheng, Y. Zhang, Y. Wei, and Y. Zhao, "Dissipative dynamics in a tunable Rabi dimer with periodic harmonic driving," *J. Chem. Phys.* **150**, 184116 (2019).

[203] F. Zheng, Y. Zhang, L. Wang, Y. Wei, and Y. Zhao, "Engineering Photon Delocalization in a Rabi Dimer with a Dissipative Bath," *Ann. Phys.* **530**, 1800351 (2018).

[204] K. sun, K. Shen, M.F. Gelin, and Y. Zhao, "Exciton dynamics and time-resolved fluorescence in aanocavity-integrated monolayers of transition metal dichalcogenides," *J. Phys. Chem. Lett.* **14**, 221-229 (2023).

[205] E.J. Heller, "Time-dependent Approach to Semiclassical Dynamics," *J. Chem. Phys.* **62**, 1544-1555 (1975).

[206] E.J. Heller, "Frozen Gaussians: A very simple semiclassical approximation," *J. Chem. Phys.* **75**, 2923-2931 (1981).

[207] E.J. Heller, "Guided Gaussian Wave Packets," *Acc. Chem. Res.* **39**, 127-134 (2006).

[208] B. Curchod, T.J. Martínez, "Ab Initio Nonadiabatic Quantum Molecular Dynamics," *Chem. Rev.* **118**, 3305-3336 (2018).

[209] G.A. Worth and I. Burghardt, "Full Quantum Mechanical Molecular Dynamics Using Gaussian Wavepackets. *Chem. Phys. Lett.* **368**, 502-508 (2003).

[210] M. Werther and F. Grossmann, "Apoptosis of moving nonorthogonal basis functions in many-particle quantum dynamics," *Phys. Rev. B* **101**, 174315 (2020).

[211] M. Werther , S. Choudhury, and F. Grossmann, "Coherent state based solutions of the time-dependent Schrödinger equation: hierarchy of approximations to the variational principle," *Int. Rev. Phys. Chem.* **40**, 81-125 (2021).

[212] D. Shalashilin and M. Child,"Basis set sampling in the method of coupled coherent states: Coherent state swarms, trains, and pancakes," *J. Chem. Phys.* **128**, 054102 (2008).

[213] A. Kirrander and D. Shalashilin, "Quantum dynamics with fermion coupled coherent states: Theory and application to electron dynamics in laser fields," *Phys. Rev. A* **84**, 033406 (2011).

[214] J. Green and D. Shalashilin, "Simulation of the quantum dynamics of indistinguishable bosons with the method of coupled coherent states," *Phys. Rev. A* **100**, 013607 (2019).

[215] G.A. Hagedorn, "Raising and Lowering Operators for Semiclassical Wave Packets," *Ann. Phys.***269**, 77-104 (1998).

[216] E. Faou, V. Gradinaru, and C. Lubich, "Computing semiclassical quantum dynamics with Hagedorn wavepackets.," *SIAM J. Sci. Comput.* **31**, 3027-3041 (2009).

[217] R. Borrelli and A. Peluso, "Quantum dynamics of electronic transitions with Gauss-Hermite wave packets," *J. Chem. Phys.* **144**, 114102 (2016).

[218] L. Chen, K. Sun, D. Shalashilin, M.F. Gelin, and Y. Zhao, "Efficient simulation of time-and frequency-resolved four-wave-mixing signals with a multiconfigurational Ehrenfest approach," *J. Chem. Phys.* **154**, 054105 (2021).

[219] L. Chen, R. Borrelli, D. Shalashilin, Y. Zhao, and M.F. Gelin, "Simulation of Time-and Frequency-Resolved Four-Wave-Mixing Signals at Finite Temperatures: A Thermo-Field Dynamics Approach," *J. Chem. Theor. Comp.* **17**, 4359-4373 (2021).

[220] D.V. Makhov, C. Symonds, S.F. Alberti, D. Shalashilin, "Ab initio quantum direct dynamics simulations of ultrafast photochemistry with Multiconfigurational Ehrenfest approach," *Chem. Phys.* **493**, 200-218 (2017).

[221] M. Ben-Nun and J. Quenneville, Ab Initio Multiple Spawning: Photochemistry from First Principles Quantum Molecular Dynamics," *J. Phys. Chem. A* **104**, 5161-5175 (2000).

[222] B. Mignolet, B. Curchod, and T.J. Martínez, "Communication: XFAIMS-eXternal Field Ab Initio Multiple Spawning for electron-nuclear dynamics triggered by short laser pulses," *J. Chem. Phys.* **145**, 191104 (2016).

[223] B. Mignolet and B. Curchod, "Excited-State Molecular Dynamics Triggered by Light Pulses - Ab Initio Multiple Spawning vs Trajectory Surface Hopping," *J. Phys. Chem. A* **123**, 3582-3591 (2016).

[224] D.V. Makhov, W.J. Glover, T.J. Martínez, and D. Shalashilin,"Ab initio multiple cloning algorithm for quantum nonadiabatic molecular dynamics," *J. Chem. Phys.* **141**,054110 (2014).

[225] G.A. Worth, and M. Robb, I. Burghardt, "A Novel Algorithm for Non-Adiabatic Direct Dynamics Using Variational Gaussian Wavepackets," *Faraday Discuss.* **127**, 307-323 (2004).

[226] L. Gao, K. Sun, H. Zheng, and Y. Zhao, "A deep-learning approach to the dynamics of Landau-Zener transitions," *Adv. Theor. Sim.* **4**, 2100083 (2021).

[227] X. Yuan, S. Endo, Q. Zhao, Y. Li, and S.C. Benjamin, "Theory of variational quantum simulation," https://doi.org/10.22331/q-2019-10-07-191.